Technical Report No.: USC-VacUV-108

1 May 1966

Contract NsG-178-61 on

Vacuum Ultraviolet and Solid State Physics

OPTICAL CONSTANTS OF SILVER AND BARIUM IN THE VACUUM ULTRAVIOLET SPECTRAL REGION

by

E. I. Fisher, I. Fujita, and G. L. Weissler

Submitted by

G. L. Weissler, Chief Investigator
Contract No. NsG-178-61

Prepared for

Office of Grants and Research Contracts
National Aeronautics and Space Administration
Washington, D.C. 20546

TABLE OF CONTENTS

Page

LIST OF ILLUSTRATIONS

LIST OF TABLES

ABSTRACT

The optical properties of evaporated silver and barium films have been investigated in the wavelength range from 1500 to 3000 Å. Reflectance measurements with unpolarized light were made at two angles of incidence, 17.5° and 72.5°, and the components of the complex index of refraction obtained from graphical solutions of the Fresnel reflection equations. The films were prepared in an ultrahigh vacuum reflectometer having a base pressure of about 5×10^{-10} torr. Radiation from a hydrogen glow discharge light source was dispersed by a normal incidence vacuum monochromator which was optically connected to the ultrahigh vacuum system by means of a sapphire window.

The energy loss functions, as computed from the optical constants, were compared with published characteristic electron loss data. The complex index of refraction of barium was fitted to a Drude model for which the plasma energy was fixed at 7.42 eV and the damping was allowed to be energy dependent.

I. INTRODUCTION

In the last two decades studies of the interaction of vacuum ultraviolet radiation with matter has become a major field of experimental physics.[1] Interest has increased in recent years because space technological advances have brought about direct contact, both human and instrumental, with pure solar radiation.[2] Thus some experimentation, such as solar emission studies,[3] were developed to study the nature of the sources of vacuum ultraviolet radiation. However, this same radiation has proven a very useful probe for investigating the nature of the material with which it is interacting. As a simple example, absorption and photoionization measurements on gases yield valuable information about the spectroscopic structure of the gas.[4]

The interaction of electromagnetic radiation with solids is an equally fruitful field of investigation. The quantities which determine the optical properties of a material are the same ones which determine many other observable quantities. Thus, optical work, in the appropriate wavelength range, can be related to phenomena such as the photoelectric effect, photo-conductivity, characteristic electron energy loss, or any other effect

which is determined by crystalline band structure. Ultraviolet radiation, which merges at high energies with x-rays and at low energies with the visible spectrum, provides a broad range which encompasses many interesting phenomena in solids. These phenomena, collectively, provide a multi-faceted frame against which the theoretician can test his models.

This work is concerned with the investigation of the optical constants of barium and was accomplished by measuring the reflectance of a plane barium surface under varying conditions of incident radiation. (As will be seen later, most work of this type is done by means of reflectance measurements.) The assumption that the nature of the first few hundred Angstroms of the material is identical to that of the bulk material is implicit in this technique. This requires, at least, that the surface be free of contamination. The present measurements were therefore carried out under ultrahigh vacuum conditions in which the minimum monolayer time[5] was 1000 seconds or more. Barium was chosen because its highly reactive nature provided a challenging material and because published data[6] indicated that this metal should have interesting optical properties in a vacuum ultraviolet range that was experimentally accessable with the available apparatus.

II. TERMINOLOGY AND TECHNOLOGY OF OPTICAL CONSTANTS

The Complex Index of Refraction

The optical properties of absorbing media may be described by a complex index of refraction

$$n' = n - ik, \tag{1}$$

where n is called the real part of the complex index and k the extinction coefficient. As for transparent media, the real part has the familiar definition

$$n = c/v, \tag{2}$$

except that v is the phase velocity of a plane wave having constant amplitude along a wave front. The extinction coefficient describes the damping of the wave as it traverses the absorbing medium and is related to the absorption coefficient μ of Lambert's law ($I = I_o e^{-\mu z}$) by

$$\mu = 4\pi k/\lambda, \tag{3}$$

where λ is the vacuum wavelength of the radiation. The absorption coefficient is proportional to the absorption cross section σ,

$$\mu = L_o \sigma, \tag{4}$$

where $L_o = 2.687 \times 10^{19}/cm^3$ is Loschmidt's number.

The complex index of refraction may generally be

substituted directly into relationships which describe dielectric media, but with a changed interpretation. For example, a modified form of Snell's law

$$\sin\varphi = n' \sin\chi, \tag{5}$$

is valid. However, the angle of refraction, χ, is now complex and the real part of the complex index is no longer simply related to the real angle of refraction. The difficulty occurs because an inhomogeneous wave, i.e., one for which the planes of constant phase are not parallel to those of constant amplitude, can exist in an absorbing medium. If a plane wave is obliquely incident upon a plane metallic surface, different points on a plane of constant phase of the refracted wave traverse different lengths of absorption path.[7] Thus, the planes of constant amplitude are parallel to the surface of the metal and those of constant phase are perpendicular to the direction of propagation of the refracted wave. This leads to the restriction on the definition of v in Eq. (2).

If Snell's law is written in the form

$$\sin\varphi = n_1 \sin\theta, \tag{6}$$

where θ is identified as the real angle of refraction, and n_1 and an associated k_1 are real quantities which describe the optical properties of the medium, then the optical constants, n_1 and k_1, become functions of the

angle of incidence φ.[8] They bear the following rather complicated relationships to the true or "normal incidence" optical constants, n and k,[9]

$$2n_1^2 = [(n^2 - k^2 - \sin^2\varphi)^2 + 4n^2k^2]^{\frac{1}{2}} + (n^2 - k^2 + \sin^2\varphi), \quad (7)$$

$$2k_1^2 = \left[\frac{n^2k^2}{n^2k^2 - (n^2 - k^2)\sin^2\varphi}\right] \times \{[(n^2 - k^2 - \sin^2\varphi)^2 + 4n^2k^2]^{\frac{1}{2}} - (n^2 - k^2 + \sin^2\varphi)\}. \quad (8)$$

A medium can be described equally well by its frequency-dependent complex dielectric constant $\varepsilon(\omega)$, which is related to the optical constants by

$$\varepsilon(\omega) = \varepsilon_1 + i\varepsilon_2 = n'^2 = (n^2 - k^2) - 2ink. \quad (9)$$

The real part of the complex dielectric constant, ε_1, is the ordinary dielectric constant usually associated with dielectric media, and the imaginary part, ε_2, is given by

$$\varepsilon_2(\omega) = 4\pi\sigma(\omega)/\omega, \quad (10)$$

where $\sigma(\omega)$ is the conductivity of the medium. There are many experimental techniques for determining metallic optical constants, or equivalently, the components of the complex dielectric constant. Some of them will be discussed in the following sections, although not

necessarily in their historical order of development.

Historical Techniques

Perhaps the most obvious approach to the optical properties of absorbing media would be the dioptric techniques common to the experimental determination of the absorption cross sections of gases or the measurement of the indices of refraction of dielectric prisms. The former would require transmission measurements on thin metallic foils. Aside from the experimental difficulties involved in producing pinhole-free and, preferably, self-supporting foils, and the problems of measuring foil thicknesses, this technique would require correction for reflections from the two surfaces of foils before any reasonable value of the extinction coefficient could be obtained. This, in itself, requires either independent reflection measurements, with a corresponding a priore knowledge of the optical constants of the foils, or measurements on several foils of varying thicknesses. Hence, simple transmission experiments can provide extinction coefficients in wavelength regions where thin metallic foils exhibit measurable transmittance.

The second of the above mentioned techniques, analagous to those used with transmitting prisms, was actually developed by Kundt[10] before the turn of the

century. He succeeded in electrolyzing very thin prisms of Cu, Pt, Fe, Bi, Au, and Ag on platinized glass and measuring the prism angles and the angles of deviation of transmitted light. Thus, he was able to calculate the index of refraction. By filtering his white light source, he was able to observe measurable dispersion in the visible spectrum for all of the metals except silver. He convinced himself that his values of the indices of refraction were truly given by $n = c/v$ by immersing his wedges in a liquid of known refractive index and measuring the change in the angle of deviation. Had his measurements been more accurate, he would, of course, have noticed the discrepancies which must have existed because of the inhomogeneous wave described by Eqs. (7) and (8).

The earliest katoptric techniques date back to Drude[11] who was active both with theoretical investigation of the optical properties of real media and with the development of experimental approaches to determine them. In Drude's method, a beam of collimated light, polarized at an angle of 45° to the plane of incidence falls on the experimental surface. The phase change between the component of the electric vector in the plane of incidence and the component perpendicular to the plane of incidence, and the ratio of the reflected intensities of these two

components are measured. This information, along with the known angle of incidence and the approximation $n^2 + k^2 >> 1$, is sufficient to calculate the optical constants[12]:

$$k/n = \sin\Delta \tan 2\psi$$
$$n = \sin\varphi \tan\varphi \cos 2\psi/(1 + \cos\Delta \sin 2\psi), \quad (11)$$

where Δ is the relative phase difference of the reflected light and ψ is the azimuth of restored polarization, i.e., the azimuth of the plane of polarization of the reflected light after it has passed through a properly adjusted Babinet compensator.

Reflectance Techniques

The usual modern experimental approach to the complex index of refraction utilizes methods which involve the measurement of light reflected from the experimental samples. All of these techniques are based upon the Fresnel equations for the reflected complex amplitude of electromagnetic radiation from the plane surface of an absorbing medium[13]:

$$r_s = \sin(\varphi - \chi)/\sin(\varphi + \chi),$$
$$r_p = \tan(\varphi - \chi)/\tan(\varphi + \chi). \quad (12)$$

If Snell's law, Eq. (5), and the substitution

$$n' \cos\chi = a - ib$$

are used, the following are obtained[8,14]:

$$R_s = \frac{(a - \cos\varphi)^2 + b^2}{(a + \cos\varphi)^2 + b^2}, \tag{13}$$

$$R_p = R_s \frac{(a - \sin\varphi \tan\varphi)^2 + b^2}{(a + \sin\varphi \tan\varphi)^2 + b^2}, \tag{14}$$

$$R_a = \tfrac{1}{2}[R_p (1 + P) + R_s (1 - P)], \tag{15}$$

$$\tan\delta_s = \frac{-2b \cos\varphi}{(a^2 + b^2 - \cos^2\varphi)}, \tag{16}$$

$$\tan\delta_p = \frac{-2 \cos\varphi[2nka - (n^2 - k^2) b]}{(n^2 + k^2)^2 \cos^2\varphi - (a^2 + b^2)}, \tag{17}$$

where

$$\begin{aligned} 2a^2 &= [(n^2 - k^2 - \sin^2\varphi)^2 + 4n^2k^2]^{\frac{1}{2}} \\ &\quad + (n^2 - k^2 - \sin^2\varphi), \\ 2b^2 &= [(n^2 - k^2 - \sin^2\varphi)^2 + 4n^2k^2]^{\frac{1}{2}} \\ &\quad - (n^2 - k^2 - \sin^2\varphi), \end{aligned} \tag{18}$$

and

$$P = (I_p - I_s)/(I_p + I_s). \tag{19}$$

The subscripts s and p refer, respectively, to those components polarized with the electric vector perpendicular and parallel to the plane of incidence. R_s and R_p are the reflectances (reflected intensities) and δ_s and δ_p are the phase shifts for the appropriate components. R_a is the total reflected intensity, taking into consideration the polarization P, as defined by eq. (19), of the incident beam. As before, φ is the angle of incidence.

The first three of the above equations (13 to 15) describe the intensities reflected from a plane surface. The next two, (16) and (17), add phase shift information. The set, therefore, completely describes all of the katoptric information which can be obtained from a metallic surface.

The general laboratory technique consists of measuring one or more characteristics of the reflection at various angles of incidence. One or more of Eqs. (13) to (17), or some combination of these equations then accurately describe the experimental situation. The appropriate equation or equations may then be considered as a set of simultaneous equations for the unknowns n and k, or possibly, n, k, and P.

As a simple example, Eq. (13) might be considered a set of two equations of the variables n, k, and φ. The reflectance R_s could be measured at two angles of incidence and, in principle, the equations solved for the unknowns $n(\varphi_1, \varphi_2, R_1, R_2)$ and $k(\varphi_1, \varphi_2, R_1, R_2)$. Or the reflectances could be measured at three different angles of incidence and the three resulting equations inverted to give $n(\varphi_1, \varphi_2, \varphi_3, R_1, R_2, R_3)$, $k(\varphi_1, \varphi_2, \varphi_3, R_1, R_2, R_3)$, and $P(\varphi_1$, etc.). Thus the experiment could also yield the polarization due to the monochromatizing apparatus, a quantity which is generally unknown for vacuum

ultraviolet instrumentation.[15] In practice, the equations cannot be inverted, and a graphical[16] inversion technique is necessary. Alternatively, it can be done by means of successive approximations using a high speed computer.[14,17,18] (As a practical matter, Hunter[14] has pointed out that the choice of R_s under these conditions would lead to almost hopelessly inaccurate values of n and k, even with very precise reflection measurements.) Humphreys-Owen[19] has indicated nine reflection methods which make use of the Fresnel reflection formulae. Unfortunately, most of these require the use of polarized incident radiation and are not easily applied to the vacuum ultraviolet region where polarizers and analyzers are inefficient or nonexistent.[20]

One of these reflection techniques, that of measuring the ratio R_s/R_p for two angles of incidence, is of considerable experimental interest. The graphical technique of inverting the Fresnel equations provides good accuracy over a reasonable range of n and k and the method has several experimental advantages. Neither the sample nor the detector need be moved between measurements of R_s and R_p, and the two readings may be taken within a very short span of time. This greatly reduces the stability requirements on the light source. Also, if the rotation of the polarizer does not

translate the incident beam from its original position on the sample, then the two reflectances, R_s and R_p, are detected using exactly the same area of the photomultiplier photocathode. Thus any variation in sensitivity across the photocathode is eliminated.[21] The main disadvantages are that one of the angles needs to be near grazing incidence (which applies also to most of the related techniques) where the reflectance is a steep function of the angle of incidence (see Fig. 1), and the ubiquitous polarizer problem which plagues workers of the vacuum ultraviolet spectral region.

All of the reflection techniques mentioned thus far have had one thing in common: In each case it was necessary to measure at least two independent quantities in order to gain sufficient information to solve the Fresnel equations for n and k.

There is a different and very important approach which requires measurement, over a broad wavelength range, of the normal incidence reflectance only. The Kramers-Kronig dispersion relations represent an integral transform[22] which relates the real and imaginary parts of any linear physical response function, such as the complex dielectric constant, the complex impedance of an a.c. circuit,[23] or the complex magnetic susceptability. As a result of the principle of causality, the two components

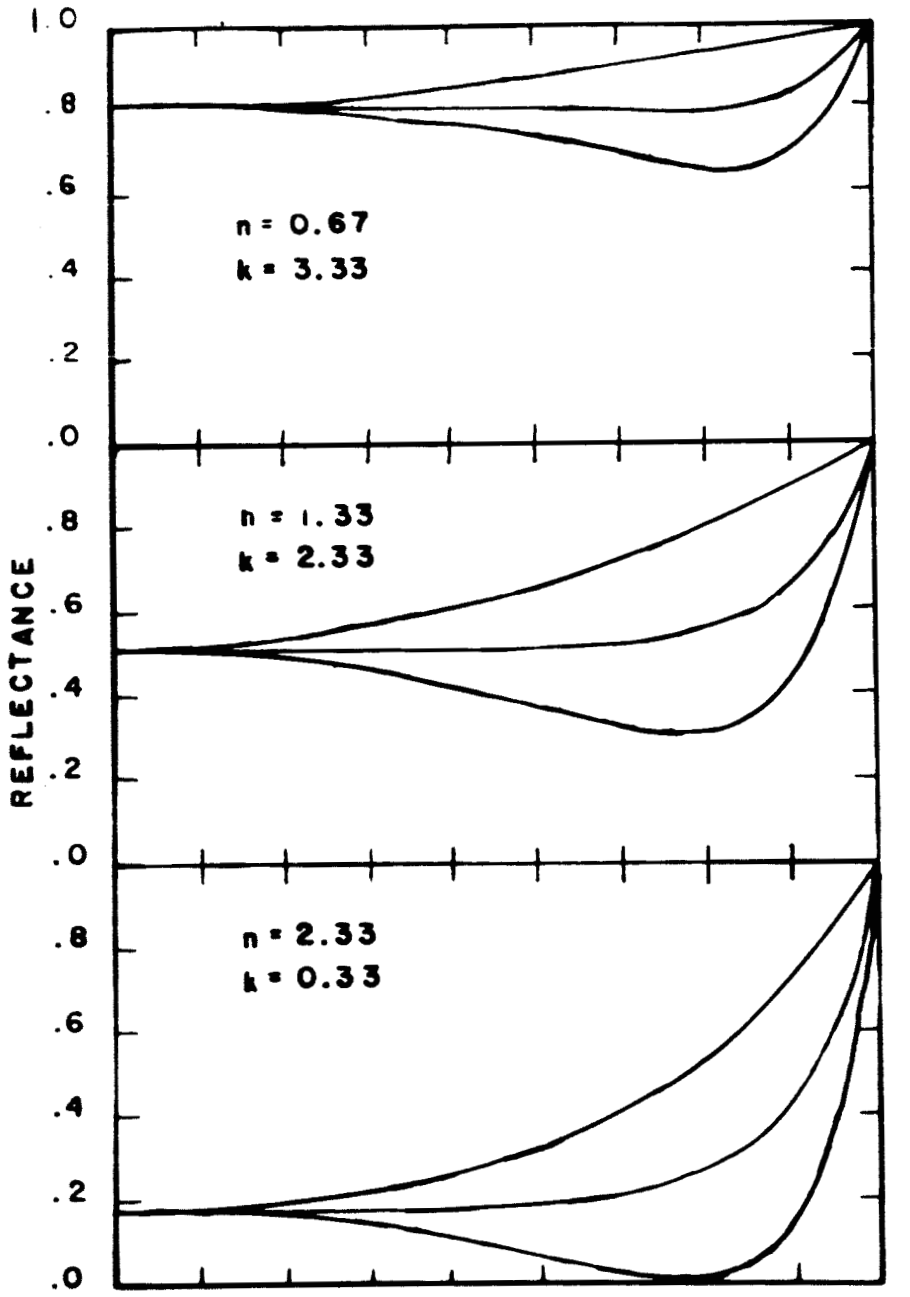

Fig. 1. Reflectance vs. Angle for Selected Pairs of Optical Constants. The upper curve is R_s, the middle curve R_a, and the lower curve R_p. For angles of incidence greater than about 70^0, the reflectance may become a very sensitive function of the geometry.

of such a function cannot be independent. If either is specified for the entire energy spectrum, then the other is determined. The Kramers-Kronig dispersion relationships provide the link between the two parts. If $Q = q_1 + iq_2$ is such a quantity, then the relations are[24]:

$$q_1(E) = (2/\pi)\ P \int_0^\infty \frac{E'\ q_2(E')}{E'^2 - E^2}\ dE' \qquad (20)$$

$$q_2(E) = -(2E/\pi)\ P \int_0^\infty \frac{q_1(E)}{E'^2 - E^2}\ dE' \ . \qquad (21)$$

The symbol P in Eqs. (20) and (21) stands for the principal value. As is evident from the limits of integration, the integrand must be known over an infinite energy range. This is, of course, impossible since the quantity must be determined by means of physical observations. However, the quadratic form of the denominator greatly reduces the contribution for values of E' far removed from E. Thus if q_1 is measured for $0<E'<E_1$, the calculated values of $q_2(E)$ will be best at low energy and be decreasingly accurate as $E' \longrightarrow E_1$. The usual technique is to extrapolate q_1 in some reasonable fashion for energies outside of the experimentally observable range.[25] This generally improves q_2 for $E'<E_1$, but is totally unreliable at higher energies.

These dispersion relations may be used to obtain

the optical constants even though the complex index does not satisfy the conditions of a linear physical response function (cf. Stern, Ref. 24). The normal incidence reflectance is measured over as wide an energy range as is experimentally feasible, and the phase calculated by means of the dispersion relations. (Any angle of incidence would fill the theoretical requirements, but would complicate data reduction since elaborate computer or graphical means would still be required to solve the Fresnel amplitude and phase equations, Eqs. (13) to (17), after an almost equally complicated numerical integration of the reflectance curve.) Also, the use of nearly normally incident radiation helps to minimize any errors which might arise from unknown polarization or the variation in the angle of incidence across the surface of the sample because of some divergence of the incident beam.[26]

The complex reflected amplitude at normal incidence is given by

$$r' = (n' - 1)/(n' + 1) = |r'|\, e^{i\theta}, \qquad (22)$$

so that

$$\ln r' = \ln|r'| + i\theta = \tfrac{1}{2}\ln R + i\theta, \qquad (23)$$

where $R = |r'|^2$ is the reflectance. From eq. (21) it can be seen that the phase is

$$\theta(E) = (e/\pi)P \int_0^\infty \frac{\ln R(E')}{E'^2 - E^2}\, dE'. \qquad (24)$$

Once the integration has been carried out, n and k may be calculated from

$$n' = (1 + r')/(1 - r') = n - ik, \tag{25}$$

so that

$$n = \frac{(1 - R)}{(1 + R - 2\sqrt{R}\cos\theta)} \tag{26}$$

and

$$k = \frac{-2\sqrt{R}\sin\theta}{(1 + R - 2\sqrt{R}\cos\theta)} \tag{27}$$

Indirect Methods

When a beam of energetic electrons is incident on a thin metallic film, it is found that some of the transmitted electrons lose energy in discrete amounts which are characteristic of the target material.[27] In some cases it is found that there are further loses in multiples of the fundamental loss. For these cases, the metal is well described by the free-electron Drude model for which the dielectric constant is given by[28]

$$\varepsilon_1 = n^2 - k^2 = 1 - \frac{\omega_p{}^2\tau^2}{(1 + \omega^2\tau^2)}, \tag{28}$$

and

$$\varepsilon_2 = -2nk = \frac{-\omega_p{}^2\tau}{\omega(1 + \omega^2\tau^2)}, \tag{29}$$

where ω_p is the plasma frequency and τ is the relaxation time associated with damping of the plasma waves. The

value of the fundamental characteristic energy loss (CEL) is then given quite accurately by the plasma energy of a noninteracting electron gas,

$$\Delta E = \hbar\omega_p = \hbar(4\pi ne^2/m)^{\frac{1}{2}}, \qquad (30)$$

where n is the electron density, e the electronic charge, and m the electronic mass. Equation (30) becomes increasingly accurate with increasing value of the quantity $\omega_p\tau$. Such metals have tightly bound core electrons and relatively free valence electrons.[29]

In other metals, the results of CEL experiments are vastly different from that given by Eq. (30). For such cases, the valence electrons are tightly bound and the presence of interband transitions serves to displace the electron loss line from the value predicted for free valence electrons, even when correction is made for the polarizability of the core electrons.[29] Some authors have related these losses to interband transitions[30] or X-ray absorption structure.[31]

The first electron energy loss experiments might be said to date back to Lenard,[32] who in 1895, using a spark as a source of electrons, investigated electron absorption in several metals as well as gaseous media. A few years later, Leithäuser[33] improved the situation by using a more homogeneous electron beam. The general nature of the losses became better known in 1924 when

Becker[34] analyzed the secondary electrons ejected by a 200 eV beam. The modern CEL experiments probably began with Ruthemann[35] who investigated collodion, aluminum oxide, beryllium, aluminum and silver. Since that time, much experimental work, both with reflected[36] and transmitted[37] electrons, has been done. In addition, the well known theoretical work of Bohm and Pines[38] provided a picture of collective electron interactions, in which the single particle excitations of the solid are drastically modified by the Coulomb interaction which exists between the valence electrons. These electrons may then be able to perform collective (plasma) oscillations having an energy considerably removed from the single particle energy differences.

In 1958 Ferrell[39] predicted that, under the proper circumstances, the plasma oscillations excited by bombarding electrons could emit electromagnetic radiation having the plasma energy. The existence of this radiation was soon verified experimentally for silver by Steinmann[40] and Brown et al.[41] The publication of these results was followed by a certain amount of literary debate[42] as to the actual origin of the radiation. The dispute seemed best resolved by Ritchie and Eldridge[43] who showed that Ferrell's result was a special case (and one that gave good insight into the physical processes

involved) of the transition radiation predicted by Frank and Ginsburg[44] in 1945 (see ref. 43 for further references), which arises when a charged particle passes from a medium characterized by one set of optical constants into one characterized by a different set of optical constants.

The above CEL and associated work are intimately related to the optical work reported here, because the cross section for the energy loss of an incident electron is proportional to the imaginary part of the reciprocal of the complex dielectric constant of the material.[45] In terms of n and k, this quantity is given by

$$\mathrm{Im}(1/\varepsilon) = 2nk/(n^2 + k^2)^2. \qquad (31)$$

Thus, if the optical constants are determined by optical means, and $\mathrm{Im}(1/\varepsilon)$ is calculated from them, then the result should be a function which has relatively sharp peaks at the energies where electron loss lines are observed. Discrepancies between data derived from these two sources have indeed motivated the pursuit, both in this research and elsewhere,[46] of ultrahigh vacuum optical experiments.

If, on the other hand, the profile of the CEL line can be accurately determined, and the resulting curve properly normalized, thus determining $\mathrm{Im}(1/\varepsilon)$ experimentally, then $\mathrm{Re}(1/\varepsilon)$ could be obtained by means of the Kramers-Kronig dispersion relations. The optical

constants n and k, could then be calculated by inverting Eq. (9), and would have been determined by an experiment which was almost independent of the condition of the sample surface.

Such an experiment has in fact been performed by LaVilla and Mendlowitz.[47] They measured the CEL spectrum of beryllium and normalized it by requiring that the following sum rules be satisfied:

$$\int_0^\infty \omega \, \mathrm{Im}(\varepsilon) \, d\omega = (\pi/2)\omega_o^2 \tag{32}$$

and

$$\int_0^\infty \omega \, \mathrm{Im}(1/\varepsilon) \, d\omega = (\pi/2)\omega_e^2. \tag{33}$$

Equation (32) is the optical sum rule and Eq. (33) the electron loss sum rule. Since the core electrons of beryllium are very tightly bound and well separated from the energy of the valence electrons, they chose the limits of integration such that only the contributions from the valence electrons could be included in the above sum rules and required that $\omega_o = \omega_e$. After successive computer-aided approximations, they achieved the desired normalization and were then able to calculate the complex dielectric constant, or equivalently, the optical constants of beryllium.

The nature of the dielectric constant in the

region of a CEL line merits some discussion. In order for $Im(1/\varepsilon)$ to have a peak, it is necessary that both ε_1 $(= n^2 - k^2)$ and ε_2 $(= -2nk)$ be small in such a manner that $Im(1/\varepsilon)$ is large. A CEL is, therefore, to be expected near an energy at which the n and k curves cross. Some authors[45] have, in fact, treated the vanishing of ε_1 as the necessary condition for a CEL. However, it is not a sufficient condition since ε_2 may not have a minimum at the same point. In general, the CEL line is expected to be at an energy slightly higher than that at which ε_1 vanishes.[48]

Some experimenters[31] have observed losses which lie lower than the plasma energy of their sample material. Ritchie[49] has identified these losses with surface plasmons which, if the metallic surface is plane and in contact with vacuum, should have an energy given by $\omega_p/\sqrt{2}$. Stern and Ferrell[50] extended the theory to include the presence of a dielectric layer on the surface of the metal. Their results retained the existence of the loss due to surface plasmons and gave the energy of the loss as $\omega_p/\sqrt{\varepsilon_d + 1}$, where ε_d is the dielectric constant of the dielectric layer. This reduces to Ritchie's result if the medium immediately adjacent to the film is vacuum. These predictions have been experimentally verified by Powell and Swan[36] as well as Wagner et al.[51]

Kanazawa[52] continued theoretical investigation of the surface waves and has shown that for a film bounded by vacuum, the surface loss should occur in a region where $\varepsilon_1 + 1$ vanishes. In analogy to Fröhlich and Pelzer,[45] he suggested that $\mathrm{Im}[1/(\varepsilon + 1)]$ should have a maximum at the energy of the lowered loss. A broad maximum of this quantity was found near the lowered loss of germanium by Sasaki.[53]

An entirely different approach to the $\mathrm{Im}(1/\varepsilon)$ spectrum was worked out by Yamaguchi[54] in 1963. He pointed out that the absorption of light polarized with the electric vector perpendicular to the surface of the film is proportional to $\mathrm{Im}(1/\varepsilon)$. He made such absorption measurements on silver and, although the ensuing calculations required prior knowledge of the optical constants, they were used only in the constant of proportionality. The experimental results yielded a peak in $\mathrm{Im}(1/\varepsilon)$ which agreed well in position and height with that calculated from independently determined optical constants, but was somewhat narrower. It is not clear which set of optical constants accurately describe silver, those determined by reflection techniques or those which could be obtained by Kramers-Kronig analysis of Yamaguchi's data. Yamaguchi suggests that discrepancies be attributed to anisotropy of the optical constants of silver films.

III. APPARATUS

General Experimental Arrangement

Since reflection measurements are, perforce, extremely sensitive to the surface condition of the sample,[55] an ultrahigh vacuum reflectometer was built in which evaporated samples could be prepared. The reflectometer is shown in Fig. 2 in conjunction with the associated monochromator and the radiation detection equipment. Four of the flanges in the optic plane of the reflectometer carry sapphire windows which transmit radiation of wavelength longer than 1450 Å. Radiation from the light source is dispersed by the grating and focused on the exit slit of the monochromator. It then passes through a sapphire window and falls on the experimental surface. This surface may be rotated, so that the incident radiation is reflected through an angle of 35° or 145°, and it may be raised so that the incident light passes undisturbed across the reflectometer and out through the window opposite the monochromator exit slit. The radiation is detected by a photomultiplier which can be interchanged between the three reflectometer exit ports.

The monochromator is pumped by an oil-sealed

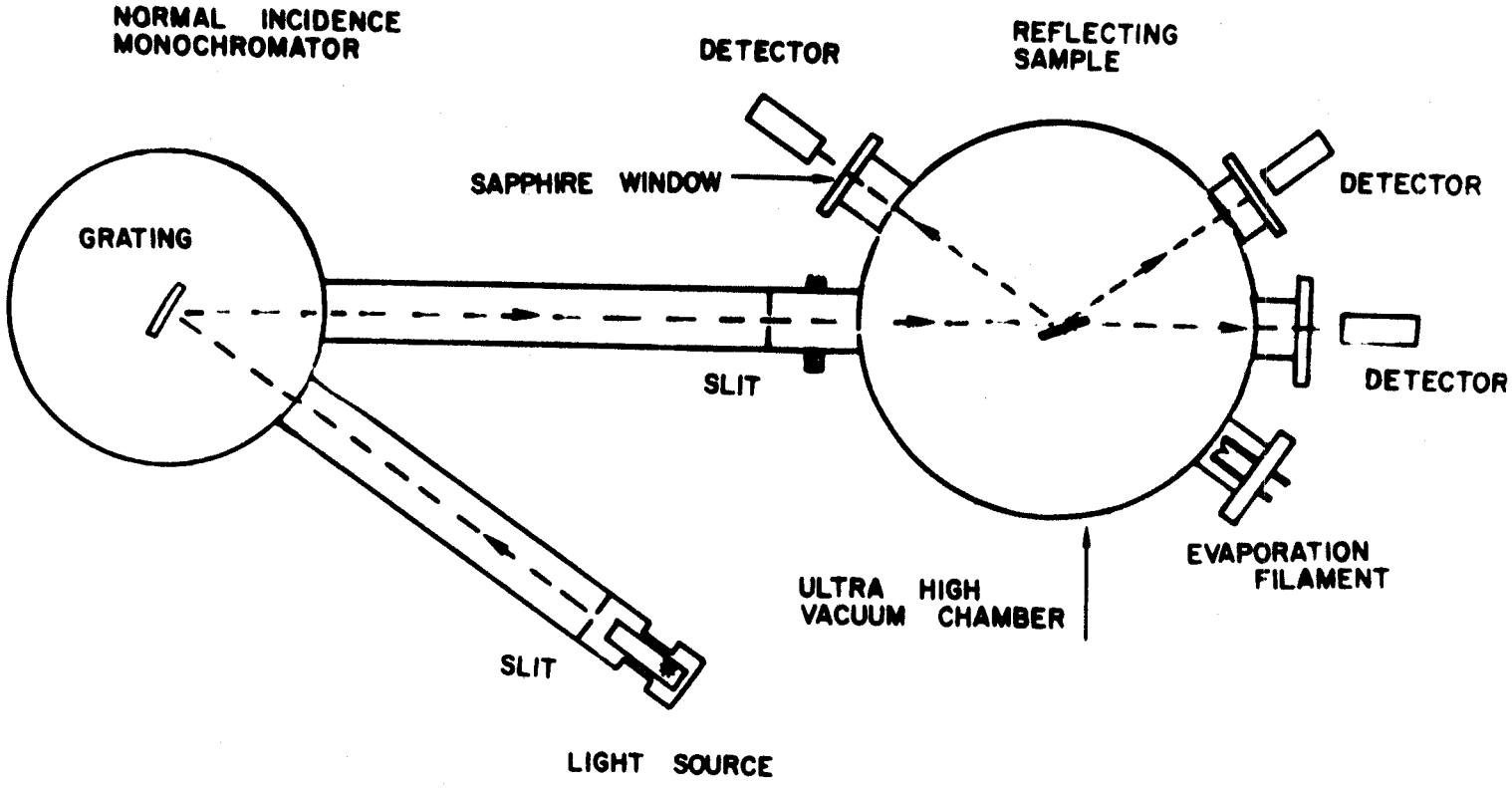

Fig. 2. Plan View of the Experimental Arrangement

rotary pump. An all-vacuum path from light source to sample is maintained by an elastomer seal between the exit flange of the monochromator and the entrance flange of the reflectometer. The sapphire window in the latter flange isolates the relatively poor vacuum of the monochromator from the ultrahigh vacuum of the reflectometer.

Reflectometer

The stainless steel ultrahigh vacuum system may be seen in Fig. 3. The system is pumped by a 1400 liter/sec oil diffusion pump. This pump is followed by a water cooled baffle (20° C), a freon cooled baffle (-40° C), and a liquid nitrogen trap (-196°C). Each of these is provided with an oil creep barrier to inhibit surface migration of the diffusion pump oil. The combination of the water- and freon-cooled baffles is optically dense as is the liquid nitrogen trap. The lower baffles are designed so as to return condensed oil to cool parts of the diffusion pump.

In addition to the oil pumping, titanium sublimators have been incorporated into the ultrahigh vacuum chamber above the liquid nitrogen trap. These consist of tungsten wires wrapped with a bifilar winding of titanium and molybdenum. When a current of 35 to 40 A is passed through these wires, titanium is sublimated onto the cold surfaces of the liquid nitrogen trap.

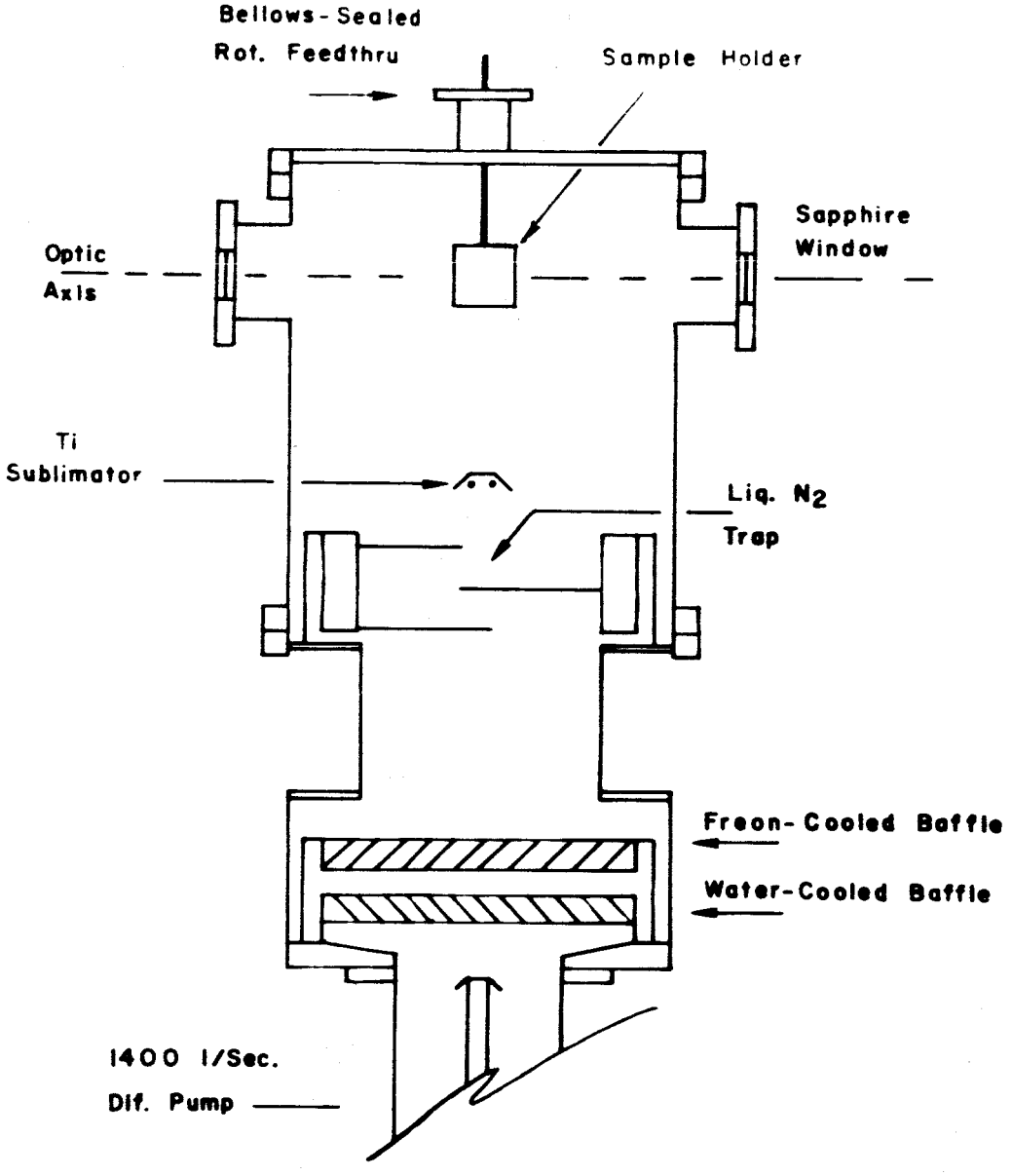

Fig. 3. Cross Section of the Reflectometer

The pumping speed of the system can thus be greatly enhanced during times of heavy gas load.[56] If currents much in excess of 40 A are used, the titanium melts and tends to form globules on the tungsten wire. This results in hot spots between the balls of molten titanium which drastically reduce the life of the filament.

The 1400 liter/sec diffusion pump is backed by a liquid nitrogen trapped 700 liter/sec diffusion pump which in turn is backed by a liquid nitrogen trapped mechanical pump. Convalex-10 oil[57] is used in both diffusion pumps. These foreline facilities provide a pressure in the 10^{-6} or 10^{-7} torr range at the outlet of the 1400 liter/sec diffusion pump.

All demountable seals above the jets of the main diffusion pump are accomplished with metal gaskets. Most of these are pinch-type seals utilizing copper gaskets.[58] The details of these seals, as they are used in the present reflectometer, have been reported elsewhere.[59] Other types of seals were used only where it was necessary to match the flanges on commercially made pieces of apparatus.

It was found that after the first few bake-outs, which were necessary for the initial set-up and testing of the reflectometer, the system was sufficiently clean to reproduce a pressure of about 5×10^{-10} torr without

further baking. This simplified the experimental procedure considerably since it meant that it was possible to make successive runs on different samples without having to remove the associated optical equipment for a bake-out. Thus the time-consuming realignment of the monochromator was avoided. The system was always vented with dry nitrogen when it was necessary to open it. When the system contamination became great enough to raise the base pressure into the 10^{-9} torr range, a 24 to 48 hour bake-out at 200° C restored it to the 10^{-10} torr range.

The substrate holder was controlled by means of a bellows-sealed rotary feedthrough mounted on the top plate of the reflectometer. A 16 pitch, $\frac{1}{4}$" lead multiple thread at the top of the holder made it possible to move the sample in and out of the optical path quickly. A keyway maintained vertical alignment. All the parts of the sample holder were machined from stainless steel; this lead to some friction difficulties which arose after the assembly had been kept under ultrahigh vacuum conditions for an extended length of time. It sometimes became impossible to rotate the sample without fear of exceeding the torque limitations of the rotary feedthrough. This situation could be alleviated by lubricating adjacent moving surfaces of the holder with molybdenum disulfide, but only with an attendant degradation (by a factor of three or four) of the reflectometer base pressure.

Monochromator

The approach chosen here toward the optical constants of metals requires radiation of known polarization. It was assumed, therefore, that the radiation was unpolarized. It was attempted to realize this condition by utilizing a 1 m monochromaotr (see Appendix I for additional design details) in which the radiation from the light source was very nearly normally incident on the grating. The angle between the entrance and the exit arms is 35°. Wavelength scans are made by simply rotating the grating (1440 grooves/mm) about a vertical axis through its center. It is used in the first outside order. Under these conditions, the angle of incidence at the grating of the undispersed radiation varies between 11.0° and 4.4° in the wavelength range between 1500 and 3000 Å.

Light Source

The light source was a water cooled dc glow discharge in hydrogen which provided a line spectrum between 1455 and 1700 Å (shorter wavelengths being excluded by the sapphire reflectometer windows) and a continuum at longer wavelengths. Although no serious attempt was made to measure the light source pressure,

it was always regulated so that the voltage drop across the 3/16" by 6" capillary was about 1.6 kV with a current of 220 to 250 mA. These parameters were sufficient to determine the operation of the source.

It was noticed that the source intensity decreased when the pressure in the hydrogen tank was less than about 300 psig and that the time-stability of the source also suffered some degeneracy. These effects were tentatively attributed to heavy impurity gases whose presence was not noticeable until the tank was nearly empty.

Detection Equipment

All intensity measurements were made with a single sodium salicylate-coated photomultiplier, type EMI 9514S, which could be interchanged between the three exit windows of the reflectometer. The photomultiplier was mounted in a light-tight aluminum housing which could be evacuated to permit the passage of wavelengths shorter than 2000 Å from the sapphire window to the fluorescent coating on the window of the photomultiplier. No absorption due to residual gas in the photomultiplier housing could be detected once the pressure was low enough to turn on the photomultiplier high voltage. The housing was fastened to the appropriate exit flange of the reflectometer by means of a set of clamps which served both to

provide sealing pressure on the O-ring and to align the photomultiplier with the optic axis.

The photomultiplier signal was amplified by an electrometer amplifier, E-H Model 201C, and recorded with a Leed's and Northrop Speedomax G, 10 mV chart recorder. A 150 μf capacitor was connected across the input terminals of the recorder in order to minimize photomultiplier noise. The photomultiplier high voltage (1.0 - 1.2 kV) was chosen to give good signal-to-noise ratio and the entrance and exit slits of the monochromator adjusted to 300μ and 480μ respectively to give full scale response for the strongest light source lines on the least sensitive electrometer range. Scanning speeds of about 130 Å/min for the line spectrum and 300 Å/min for the continuum were chosen so that lines below 1700 Å were not distorted because of the recorder response, which was somewhat degraded by the above mentioned capacitor.

The sodium salicylate coating for the photomultiplier was applied with a homemade atomizer. It was attempted to reproduce 1.4 mg/cm^2 density recommended by Masuda and Seya.[60]

Evaporator

The evaporator was installed in the optic plane of the reflectometer. It consisted of six 200 A ceramic

insulated, electrical feedthroughs welded into a demountable stainless steel flange. The conductors were arranged so that a total of three evaporation boats could be installed. The sample material was evaporated from either 0.005" wall thickness tantalum boats or from coiled baskets made from 3 x .030" multistrand tungsten wire.

A copper shield surrounded the evaporator and protected the rest of the system from material which was evaporated in random directions. A shutter mounted behind the substrate holder was large enough to intercept all evaporant which passed the substrate during sample preparation. It could also be positioned so as to protect the substrate surface from the evaporation filament during out-gassing procedures.

Prior to loading, the evaporator was cleaned by washing first in water, then in acid, and finally in clean acetone. In the case of barium, the oxides were scraped off in a helium atmosphere before the acetone cleaning. This helium atmosphere was maintained as much as possible during the loading operation, and the system pumped out as quickly as possible.

IV. EXPERIMENTAL PROCEDURE

Measurements

The sample material was loaded into the evaporator and outgassed after the system pressure had reached the ultrahigh vacuum range. The outgassing process was repeated until it was possible to obtain a slight evaporated deposit on the back side of the shutter without seriously exceeding ultrahigh vacuum pressures. The system was allowed to recover to its base pressure before attempting to produce an experimental surface. The evaporation was then made as quickly as possible, the time usually amounting to less than five seconds. During the later evaporations, the titanium sublimators were operated continuously. The pressure inevitably rose to the 10^{-5} or 10^{-6} torr range, but dropped back to the ultrahigh vacuum range within a few seconds.

The usual procedure for a new film was generally as follows. The light source was started and allowed to run for two or three hours in order to stabilize. An initial measurement of the incident intensity (I_o) was made before the evaporation. The substrate was then lowered into the range of the evaporator, but shadowed

by the shutter. The evaporation boat was heated until a slight deposit was visible on the shutter. The substrate was immediately rotated into position in front of the evaporator and the evaporation current increased to a previously determined maximum value. This value varied somewhat from experiment to experiment, depending apparently upon the amount of material loaded into the evaporation boat and perhaps upon minor variations in the evaporator geometry which occurred when it was assembled. In any case, this maximum evaporation current produced a film which was opaque to visible light in a few seconds. Chemical analysis later indicated that the film thicknesses ran from 2000 to 3000 Å.

Even though the evaporator was designed to carry two or three boats, there was only one substrate available. It had been hoped that several experimental surfaces could be evaporated successively. This turned out to be difficult. If a new film of barium was evaporated on top of an old one, the new film usually gave every appearance, both visually and in its interaction with ultraviolet radiation, to that of a film which had been stored for a week or more under high vacuum conditions. It would have a grey appearance, probably the same milkiness reported by O'Bryan[61] or the "bloom" mentioned by Maurer.[62] In one case, an attempt was made to evaporate

a silver film on top of an old barium film. The silver film started to peel off immediately.

After the evaporation was complete, the grating in the monochromator was rotated so that the central image was focused on the exit slit. The new film was then oriented so that the bright, visible central image was centered on the normal incidence exit window. Two measurements were then made of the intensity reflected at 17.5° (I_n). The central image was again focused on the exit slit and the sample rotated so that the beam reflected at 72.5° was centered on the grazing incidence exit window. Two measurements of the intensity reflected at this angle (I_g) were then made. A second measurement of I_o was made, and then the whole process repeated so that for a new film, the sequence was as follows: I_o, I_n, I_n, I_g, I_g, I_o, I_n, I_n, I_g, I_g, I_o. The first six measurements were considered to be the first run on that particular film and the last six the second run on the film. The middle I_o was used as a common check on the light source intensity for both runs. In this way, at least two (and sometimes, when time permitted, three) complete reflectivity runs, at two angles of incidence, were made on each fresh film. After the initial runs on a fresh film, further runs were made on ensuing days so that aging effects during storage of the film could be observed.

Data Reduction

The main difficulty in reducing the experimental data was caused by the existence of a large percentage of scattered light in the output of the monochromator. This was attributed partially to the high intensity of the hydrogen continuum and partially to a grating of doubtful quality. This undesired background radiation was subtracted from the total signal through the use of two filters which could be inserted between the light source and the grating. One of the filters was glass, opaque for $\lambda < 2900$ Å, and the other was potassium chloride, opaque for $\lambda < 1750$ Å.

Insertion of a filter, say KCl, gave a background level that clearly consisted only of wavelengths longer than 1750 Å. Fortunately most of the stray light did come from the continuum, but it was still necessary to correct for that having shorter wavelength.

The scattered light was, of course, most intense when the shorter wavelengths were focused on the exit slit. For I_o, the fraction with $\lambda_{scat} < 1750$ Å was small enough that for two adjacent lines it was reasonable to make the following approximation,

$$\frac{I_o(\lambda_1) + I_{os}}{I_o(\lambda_2) + I_{os}} = \frac{I_o(\lambda_1)}{I_o(\lambda_2)} , \qquad (34)$$

where $I_o(\lambda_1)$ and $I_o(\lambda_2)$ are pure light intensities for $\lambda_1 \doteq \lambda_2$ and I_{os} is the scattered component consisting of wavelengths shorter than 1750 Å.* For the normal incidence reflectance measurements, the scattered light accounted for a much larger part of the total signal, because the reflectance for the pure light was very low (about 1% for old films) at 1450 Å but increased for longer wavelengths. Thus, the stray light was not as strongly modulated by the reflectance curve as the pure light. As a result, the scattered light having wavelengths shorter than the KCl cutoff made a large contribution to the total signal at 1450 Å and could not be determined by inserting the filter.

Since both the reflectance and the scattered component seemed to be smoothly varying functions of wavelength, the total scattered component at short wavelengths was found by demanding that the ratio of adjacent line heights be the same for I_n as it was for I_o. That is, for the reflected data at short wavelengths, the following was assumed to be true and was solved for I_{ns},

$$\frac{I_n^{ts}(\lambda_1) - I_{ns}}{I_n^{ts}(\lambda_2) - I_{ns}} = \frac{I_o(\lambda_1)}{I_o(\lambda_2)} . \qquad (35)$$

Here $I_n^{ts}(\lambda_1)$ is the total normal incidence signal at λ_1 and the quantity $I_n^{ts}(\lambda_1) - I_{ns}$ represents the pure light reflected at normal incidence.

In this line spectrum region, the background was obtained by interrupting the monochromator scanning and inserting the KCl filter between the lines at which the data were taken.

For longer wavelengths, i.e., when scanning the continuum, the scattered light longer than 1750 Å was passed by the KCl filter but absorbed by the glass filter. That is, insertion of the KCl filter gave a background which also contained most of the true signal and insertion of the glass filter yielded a background that did not include the scattered light between 1750 and 2900 Å.

The technique for determining the background in this wavelength region is indicated schematically in Fig. 4, which may be considered to represent a strip chart containing a single scan of the spectrum with the various background levels added. It was observed that, in the range where the KCl filter was opaque, the intensity of the stray light seemed to be a function which decreased approximately linearly with increasing wavelength. This was also true of the glass background. It was also found that if the KCl level was extrapolated to longer wavelengths, it intersected the glass level at the transmission edge of the glass filter. Therefore, the valid signal was assumed to be the difference between the total signal and the extrapolated KCl level. This is equivalent

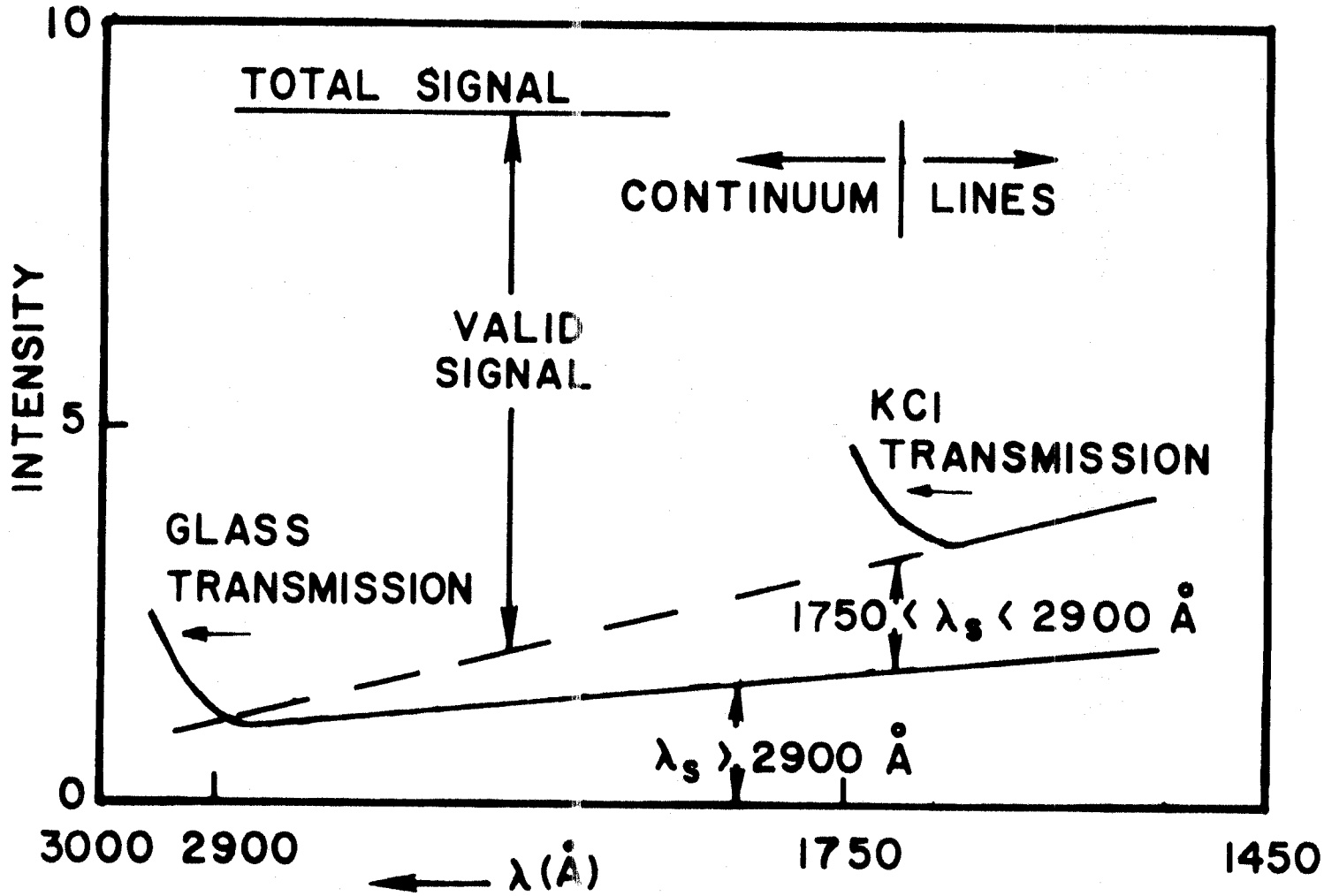

Fig. 4. Scattered Light Subtraction Method. The lower curve is light transmitted by the glass filter, the second curve is that transmitted by the CKl filter. The continuum is represented schematically by a straight line.

to the assumption that the scattered component of the output intensity consists only of wavelengths longer than the wavelength focused on the exit slit. The contribution of the scattered light was negligible beyond 3000 Å.

In practice the background in the continuum region was obtained by measuring the KCl level just short of the KCl transmission edge. During the scan of the continuum, the glass filter was inserted occasionally. This level was then extrapolated to 2900 Å and a line drawn from the last measured KCl level so that it intersected the glass level at this wavelength. The continuum was interpolated across the gap caused by insertion of the filter when necessary to obtain a datum point.

After the data were obtained in the above manner from the strip charts, a computer was utilized to expedite the rest of the data reduction (the Fortran programs are listed and explained in Appendix II). As was indicated in the preceeding section of this chapter, each run consisted of six measurements in the spectral range appropriate to the experimental material; two each of I_o, I_n, and I_g. The computer averaged the corresponding intensity pairs, printed out the precision (in order to give a measure of the light source stability), and then calculated the reflectances at the two angles of incidence.

The reflectance values delivered by the computer

were then used to obtain the optical constants from curves similar to those shown in Fig. 5. These are curves of constant n and constant k plotted in the $R(17.5^{\circ})$, $R(72.5^{\circ})$ plane. For each datum point a line drawn vertically from the abscissa intersects a line drawn horizontally from the ordinate. The positions of these lines are, of course, determined by the pair of reflectances. Through the intersection of these two lines will also be (in principle) one curve of constant n, and one curve of constant k. This n and k pair then corresponds to the given reflectance pair. The curves actually used for the data reduction were drawn on a much larger scale and with a much higher density of n and k curves. In practice, the optical constants had to be determined by interpolation between the appropriate curves. The program used to generate these curves is explained in Appendix II.

The optical constants thus obtained were punched into a second deck of IBM cards and a third (again, see Appendix II) program was used to calculate the complex dielectric constant ε, the energy loss function $\mathrm{Im}(1/\varepsilon)$, and the surface loss function $\mathrm{Im}[1/(\varepsilon + 1)]$. These results were plotted separately so that any changes due to aging of the film should not be masked by an averaging procedure.

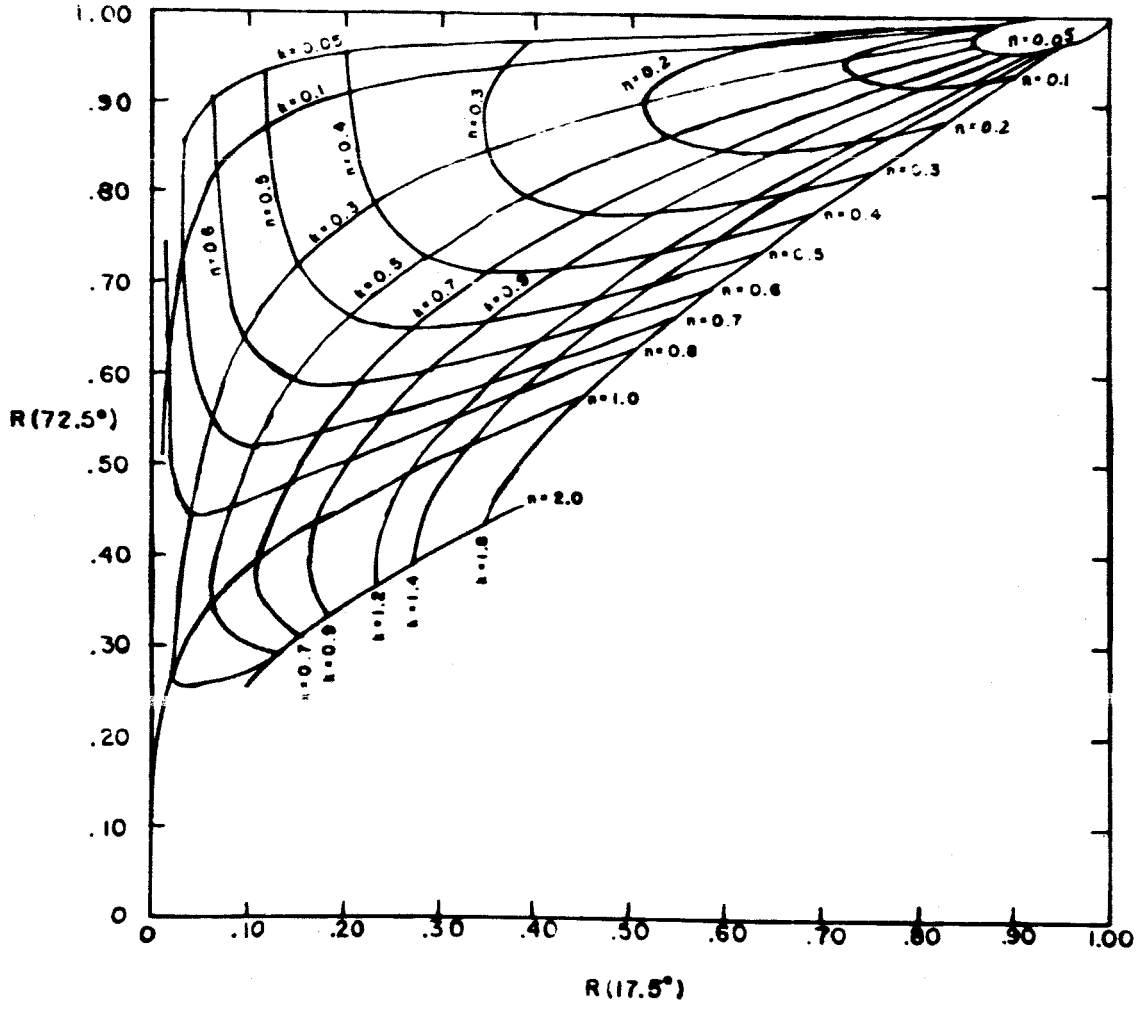

Fig. 5. Curves of Constant n and k in the R_n, R_g Plane. The curves represent the transformation from R-space to n,k-space.

V. EXPERIMENTAL RESULTS

The primary purpose of this work was the investigation of the optical properties of barium. However, since the equipment employed was new and untried and since the experimental material was itself difficult and relatively unexplored, it was felt that a certain amount of repetition of older work was justified. Therefore, a short presentation of reflectance reults obtained with silver is also included in this section.

Silver

The reflectance data and the optical constants of silver are shown in Fig. 6 and the associated energy loss function in Fig. 7. The results shown in these figures agree qualitatively with previous work.[63] The sharp rise in the reflectance at the plasma energy and the accompanying minimum of the extinction coefficient and the drop in the real part of n' are gratifyingly similar to the known properties of silver. The energy loss function shows the familiar sharp peak at 3.8 eV as well as a secondary broader maximum at about 8 eV which has been observed by some of the experimentalists of Ref. 62.

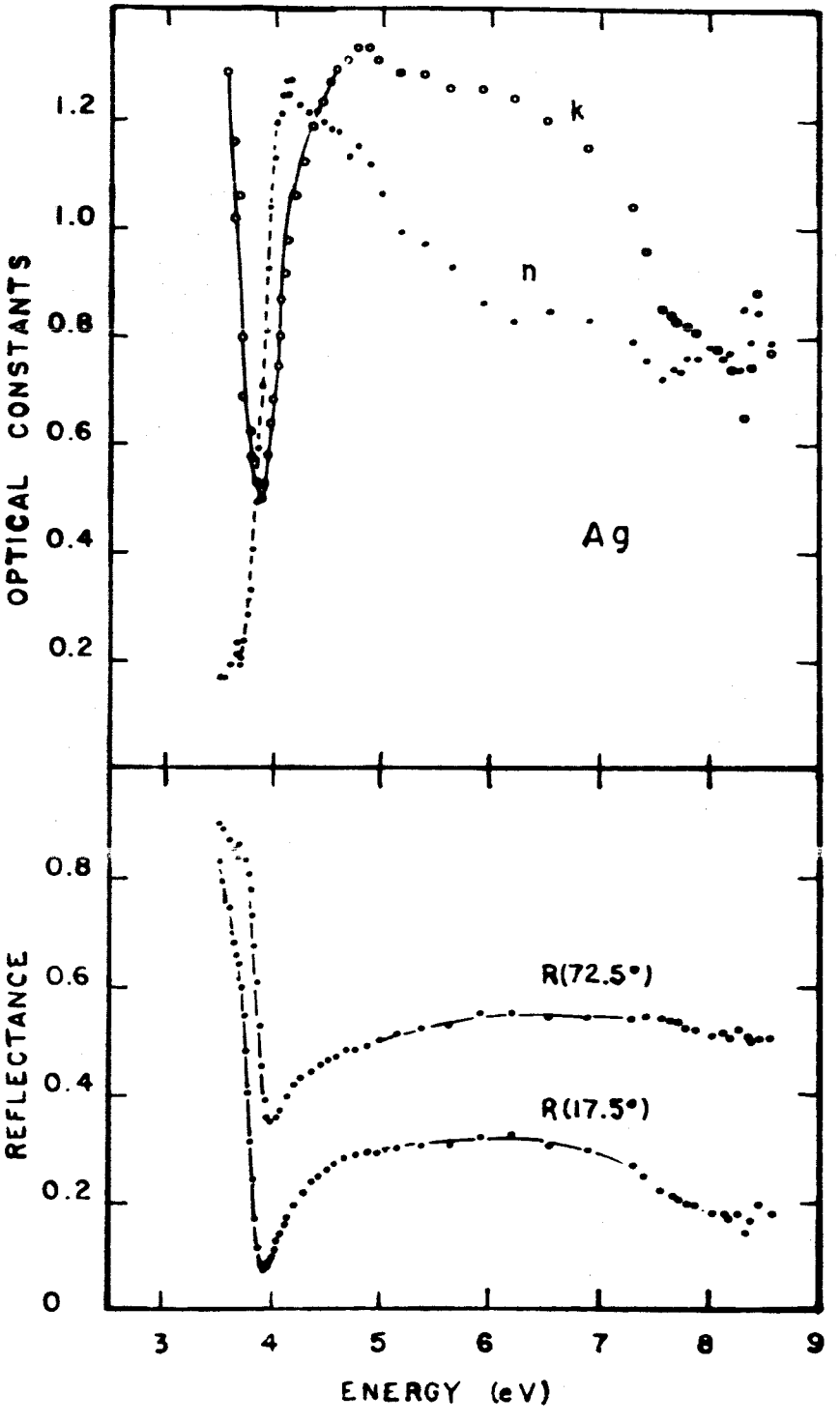

Fig. 6. Reflectance Data and Optical Constants of Silver.

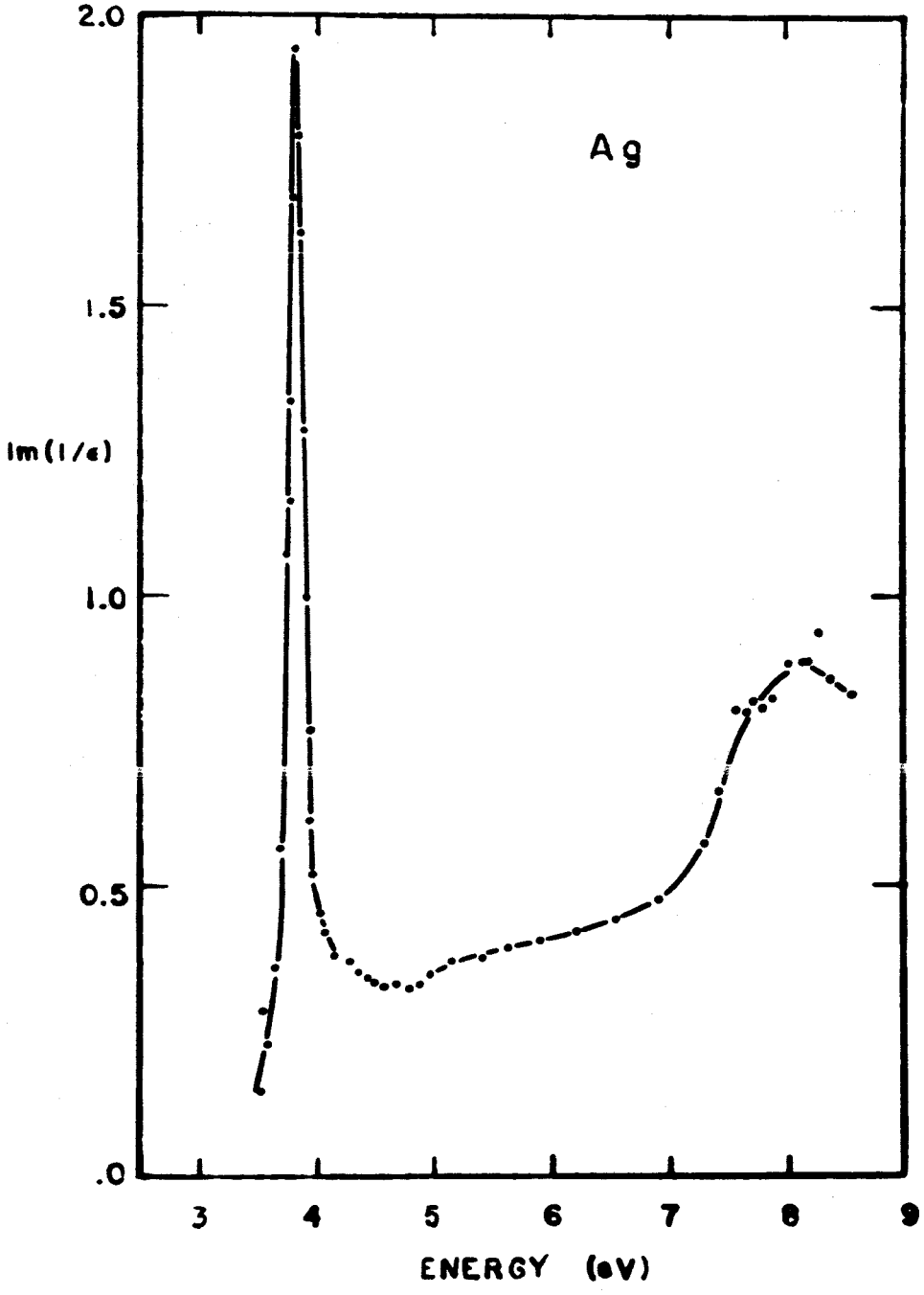

Fig. 7. Energy Loss Function for Silver

The quantitative discrepancies between these data and those of Ref. 62 are attributed to some of the scattered light difficulties explained in the previous chapter. Corrections for these errors have been made in the barium data to be presented in the next section.

No attempt was made to fit the silver data to a theoretical model since the plasma energy is determined almost entirely by interband transitions and would require extensive band calculations on a material which has already been well studied. The free electron model yields a plasma energy of 9.2 eV, an energy which is removed by nearly an order of magnitude from the experimental value.

No data are presented for longer wavelengths because the higher reflectances there required that the optical constants be obtained from the upper right hand corner of Fig. 5. In this region, the k curves are very sensitive to the normal incidence reflectance and a reflectance error of less than 1.0% can change the extinction coefficient by a factor of three or four. The experimental precision was not good enough to yield meaningful data at energies much below the plasma energy.

Barium

A typical set of reflectance curves for the barium films is shown in Fig. 8. The optical constants

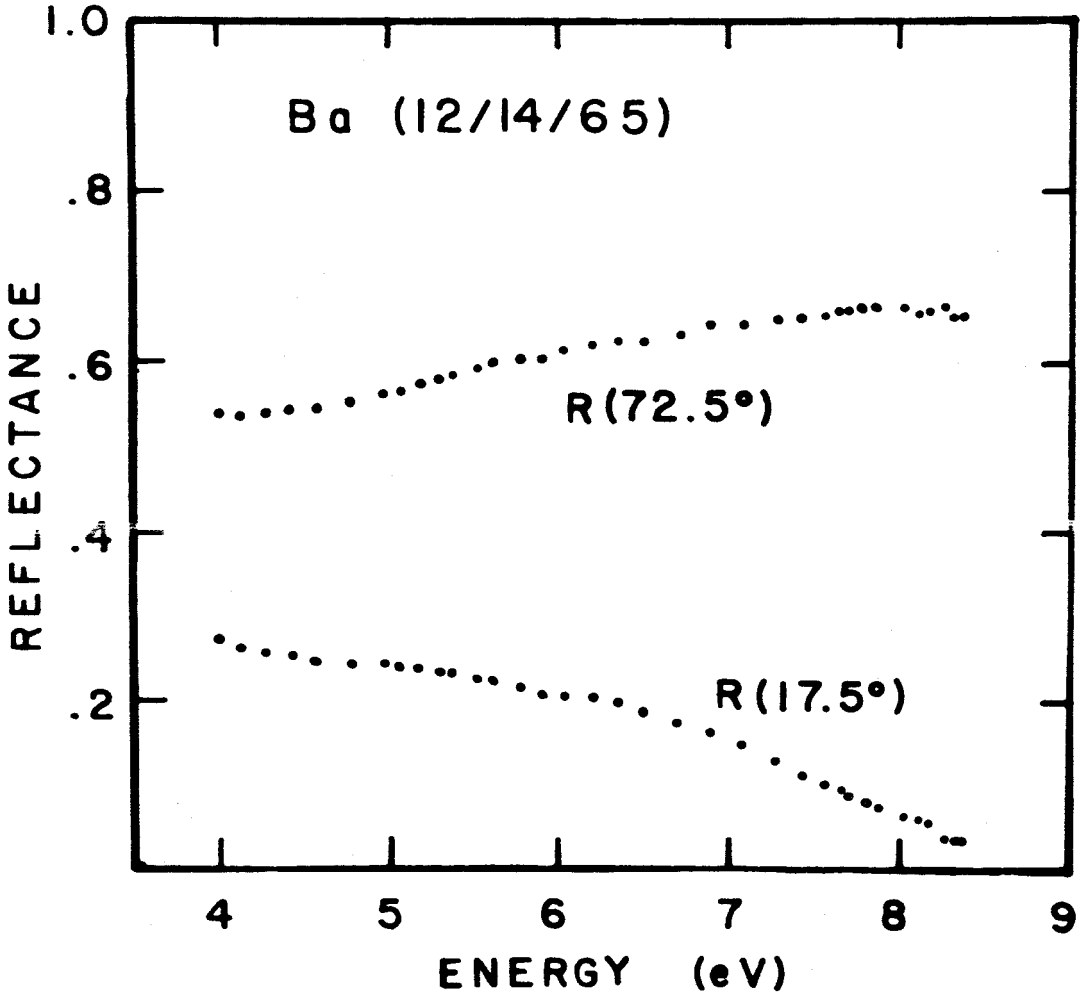

Fig. 8. Reflectance Data for Barium

are displayed in Fig. 9 and the energy loss functions in Fig. 10.

There is little to be noted in Fig. 8 except for the precision of the reflectance measurements and the general trend of the reflectance data, i.e., the respective increase and decrease of R_g and R_n with increasing photon energy.

The solid curves in Fig. 9 represent the present results. As can be seen, they match the dotted curves which were obtained from Ref. 62. The downward arrow indicates the plasma energy as reported by Robins and Best.[6] This value may also be obtained from Eq. (30) if the bulk barium density is used along with the assumptions that there are two valence electrons per atom and that the effective electronic mass is equal to the free electron mass. As will be seen later, this value does not agree with the present work.

The upper curve in Fig. 10 is the CEL function for barium as obtained from the optical constants shown in Fig. 8. The peak of the function is distinctly higher than the CEL reported by Ref. 6. The lower curve is the surface loss function. The peaks of these functions agree well with the relation

$$\omega_s = \omega_p/\sqrt{2} \ , \qquad (36)$$

where ω_s is the frequency of the surface loss. These

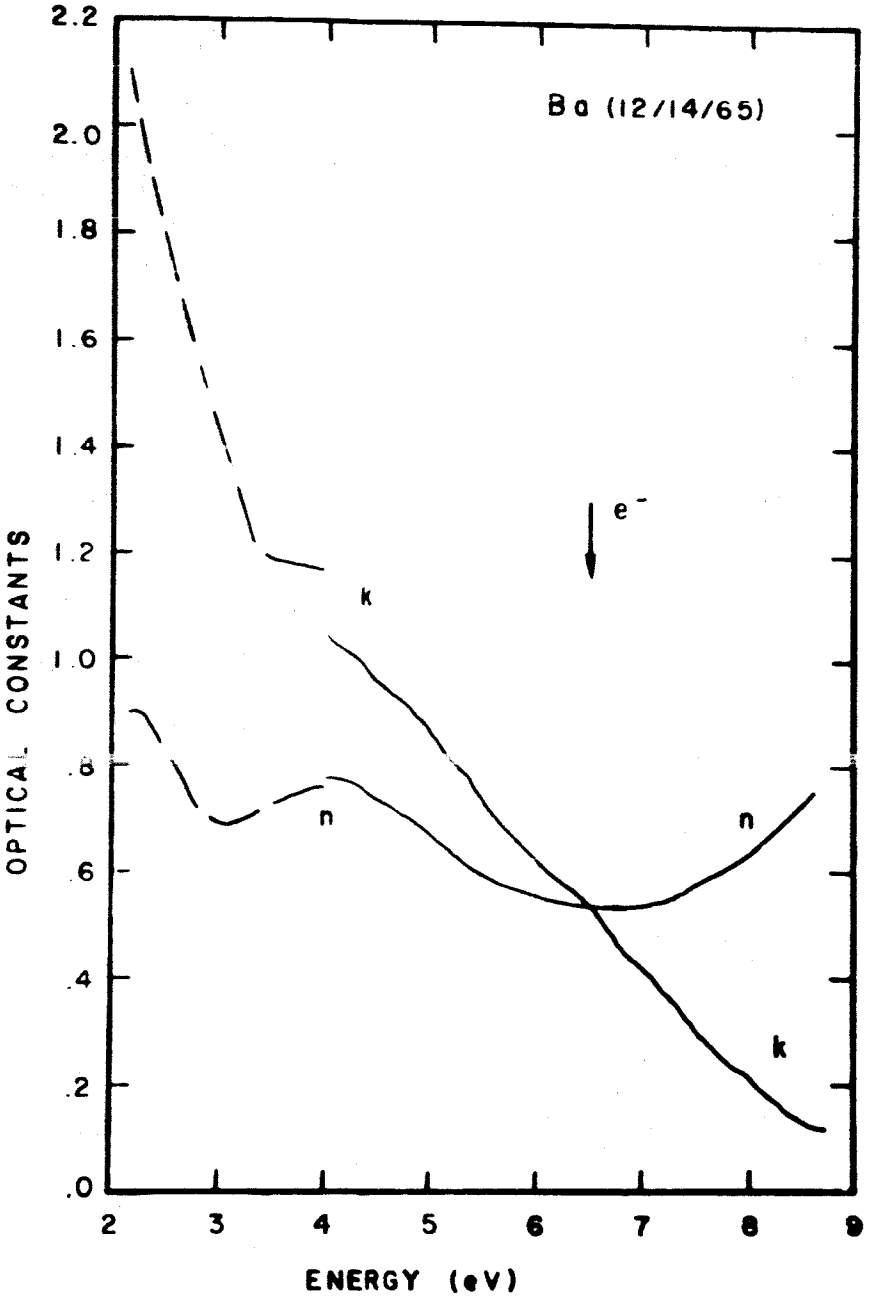

Fig. 9. Optical Constants of Barium. The solid curves represent the present work and the dashed curves the work of Ref. 62.

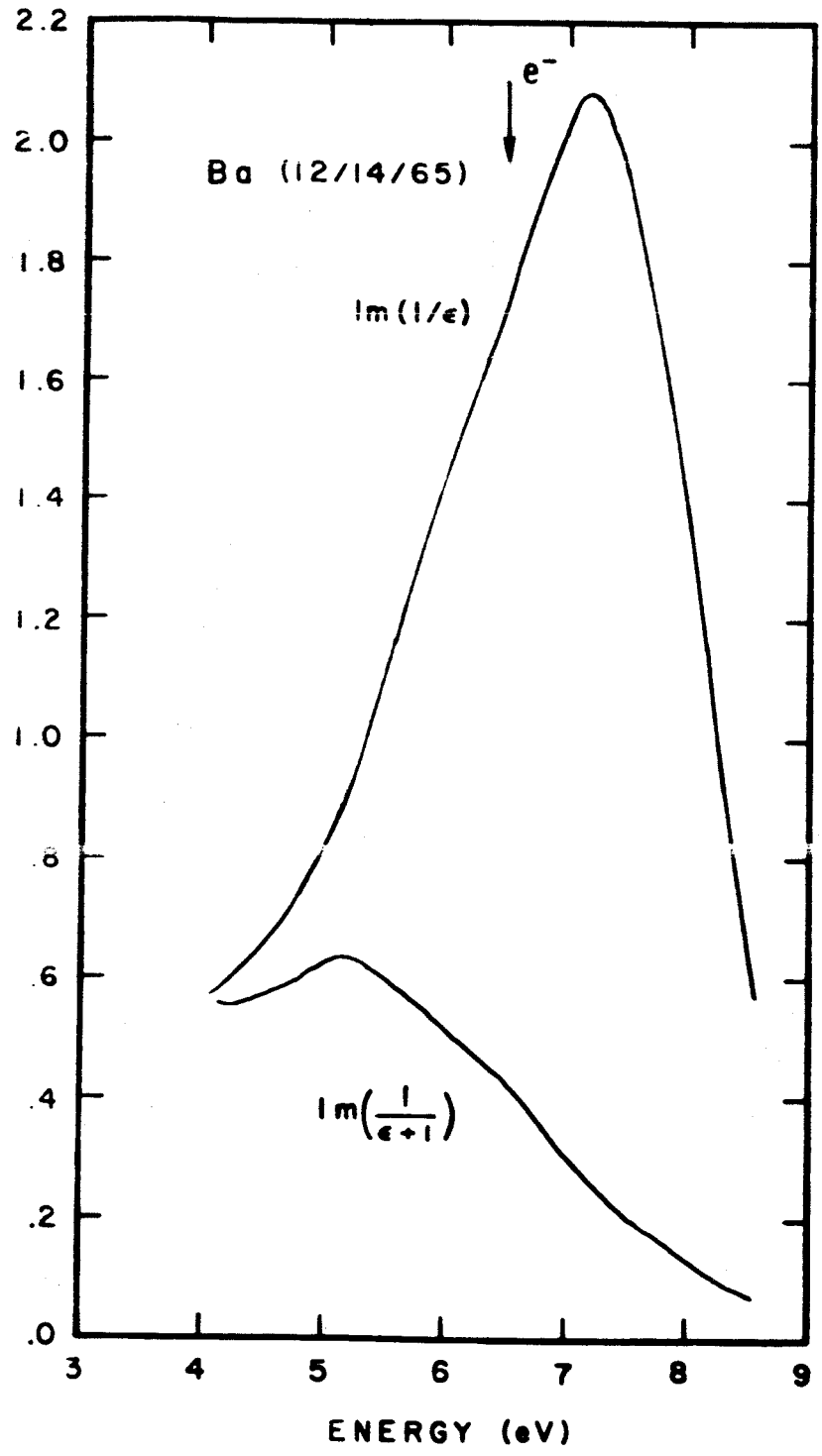

Fig. 10. The Energy Loss Functions for Barium. The upper curve is the bulk loss and the lower curve the surface loss.

CEL functions bear little resemblance to those reported by Rudberg[64] in 1936.

After crude calculations, it was found that the present barium data bore a remarkable resemblance to the simple Drude model of metallic optical properties. Therefore, it was attempted to fit the present work to the Drude model using a fixed value of the plasma energy but allowing the relaxation time τ, to be frequency dependent.

As can be seen from Fig. 11, in which the solid curves are a duplication of the experimental curves of Fig. 9 and the circles represent points on the fitted theoretical curve, a very good fit was obtained. The plasma energy corresponding to these circles is 7.415 eV, nearly one electron volt higher than that reported by Robins and Best.[6] The corresponding energy dependence of τ is seen in Fig. 12 where a maximum near 6.5 eV is clear.

It seems worth noting that the present n and k curves cross ($\varepsilon_1 = 0$) at 6.5 eV, an energy which has been reported as the CEL for barium.[6] As has been mentioned before, this condition has been considered sufficient to define the plasma energy. However, this is only true with no damping of the plasma waves. The actual shift of the plasma energy from the crossing point of the n and k curves is determined by the magnitude of the relaxation time τ.

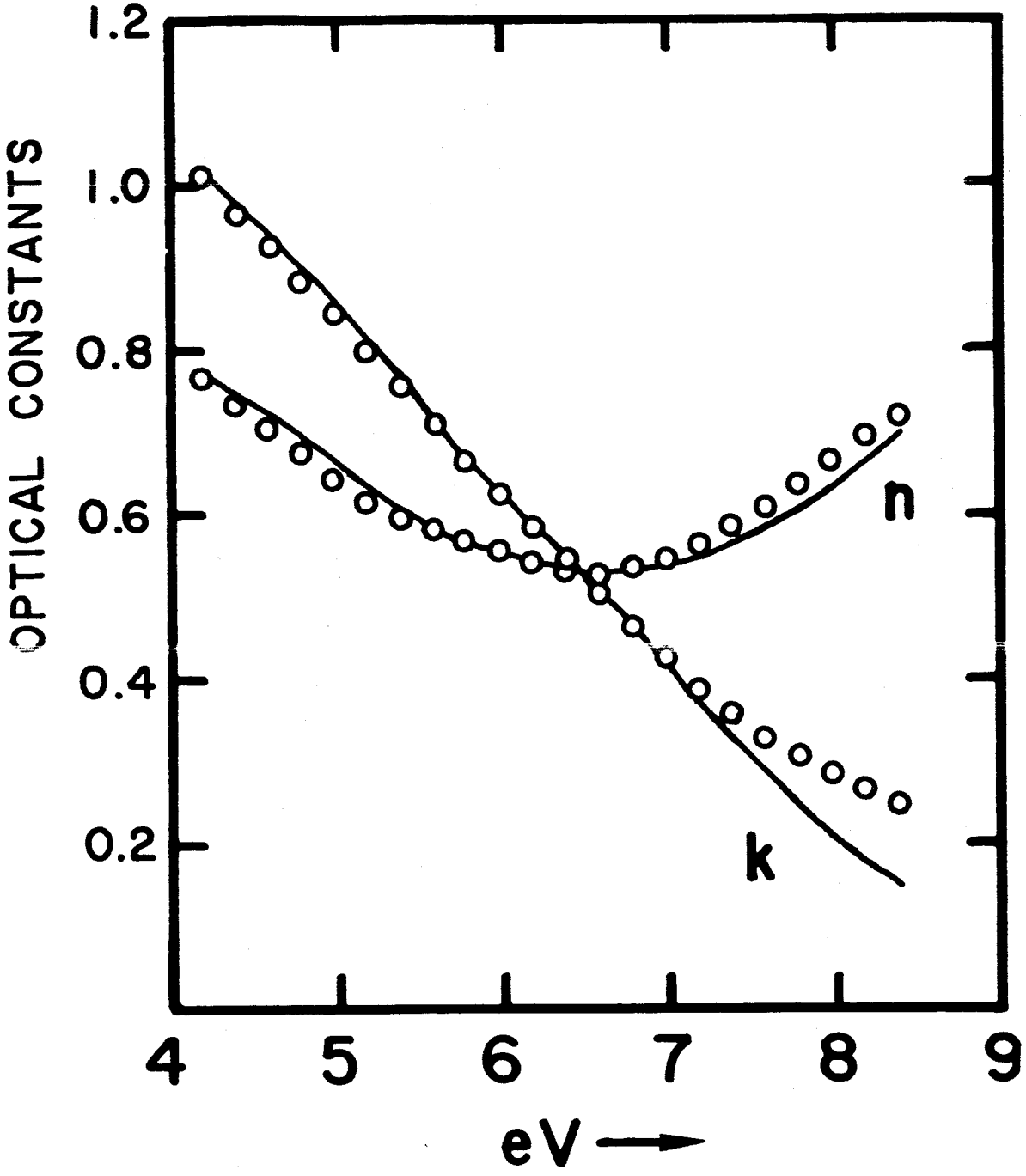

Fig. 11. Comparison of Experimental Data with the Drude Model. The solid curves are the same as those of Fig. 9. The circles represent the fit of the theoretical curve to the experimental data.

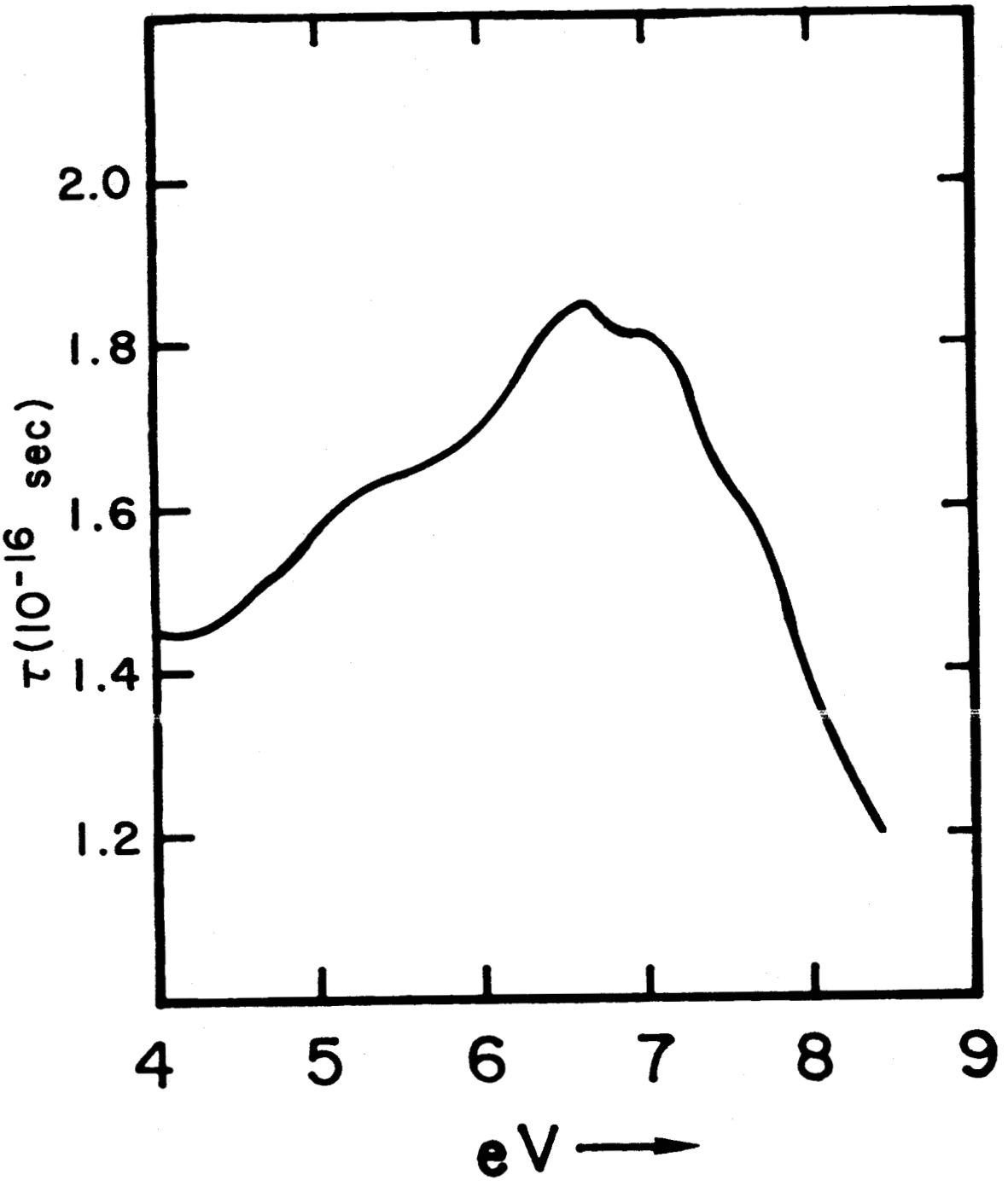

Fig. 12. Energy Dependence of the Relaxation Time for the Curve Fitting Shown in Fig. 11.

As a check, a second fit to the Drude model was made using the experimental data between 6.0 and 7.5 eV. For this narrower energy range, the fit to the Drude optical constants was, of course, somewhat better, but the general results did not differ significantly from those shown in Figs. 11 and 12.

As the barium films were allowed to age in the ultrahigh vacuum system, a slight rise in the reflectance was observed during the first 24 hours. This increase cannot be explained, certainly no interference effects were observed in the experimental wavelength range. As the films continued to age, the reflectance decreased monotonically, the normal incidence reflectance being the most sensitive. During this process, the peak of $\mathrm{Im}(1/\epsilon)$ became broader and flatter and tended to move toward lower energies until it disappeared altogether.

APPENDIX I

MONOCHROMATOR DESIGN

Rowland invented the concave diffraction grating in 1882 when the vacuum ultraviolet was suffering developmental birth pangs.[65] This grating is now the heart of most of the ultraviolet instrumentation in the world. The first really complete theoretical treatment of the concave grating was given by Beutler[66] in 1945. Beutler's approach was later examined critically and improved upon by Namioka[67] who found some errors and vagueries in Beutler's theory (references to the development of grating theory are listed copiously in Ref. 67).

The concave grating served well in vacuum spectrographs, but soon the development of photoelectric detecting devices lead to the desire to build monochromators, that is, to build instruments in which a variable band of nearly monochromatic light could be made available at a fixed position (in contrast to spectrographs, which are highly appropriate for photographic detection, but in which the various wavelengths appear at different physical positions). Many such devices have been constructed, including some which are

similar to that of the present work. There is no desire here to try to summarize them. However, it is worthwhile to mention the design of Seya,[68] partially because it seems to be the leading monochromator and partially because it is at least mechanically similar to the present monochromator in that the slits are fixed and the only motion of the grating is rotation around a vertical axis through its center.

Many of the previous monochromator designers had maintained a geometry in which the grating and the entrance and exit slits stayed on the Rowland circle. This necessitated complicated and bulky mechanical arrangements which were difficult to apply to the vacuum ultraviolet. Seya sought a geometry in which the slits could be fixed, although not necessarily on the Rowland circle, and in which the only grating motion was a simple rotation.

Seya's technique then was to apply Fermat's principle to the light path function[66] and to look for a solution which fulfilled the requirements of his desired geometry and yet provided good focus over a broad wavelength range. He found that if the angle subtended at the grating by the two slits was $70^{\circ}15'$, he could maintain excellent focus even with a grating excursion of several degrees (see Fig. 13). For a one-meter grating, the slits should be about 82 cm from the grating.

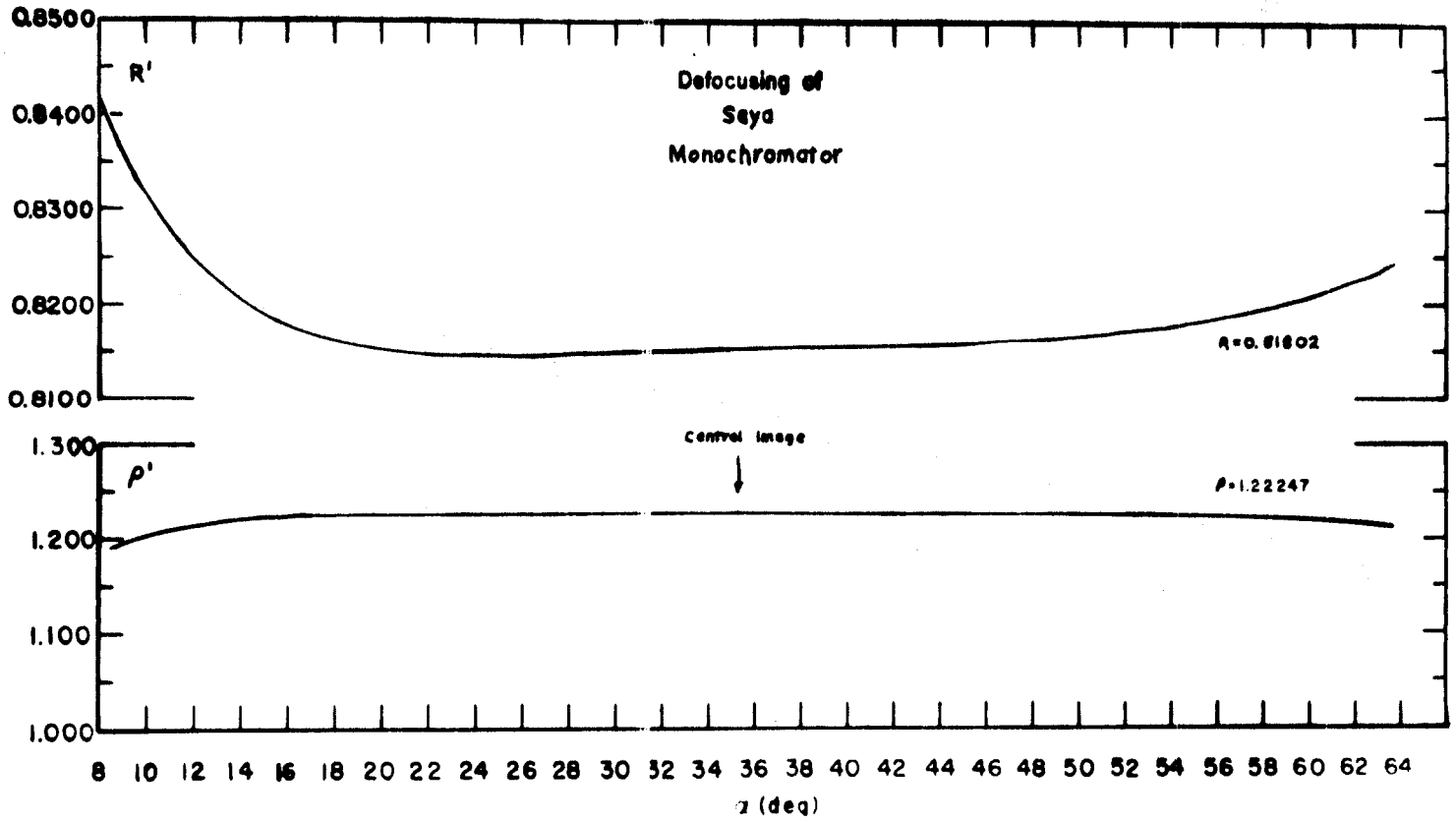

Fig. 13. Defocusing of the Seya Monochromator. For a one-meter grating, the upper curve represents the distance from the grating to the focused image. The lower curve is the reciprocal of the upper curve and may be compared with those of Fig. 12 which are drawn to the same scale (1/10 that of the upper curve in this figure).

For the present work, the focus requirements on the monochromator were not very stringent, but the state of polarization of the emergent light was significant. At the time the equipment was being designed, it was suspected that a fair degree of polarization might exist in the Seya geometry. Therefore, it was decided to construct a monochromator in which the light from the entrance slit was nearly normally incident upon the grating, thus minimizing polarization by reflection at the grating. (This suspicion has since been justified by Rabinovitch et al.[69] who investigated the polarizing characteristics of the Seya monochromator.) The angle between the entrance and exit arms was chosen to be 35° (see Fig. 2), an angle which was compatible with the associated apparatus and yet left sufficient flexibility to convert the monochromator to a Seya if it were to be used later in some other application.

The following equations apply to any concave grating mounting,

$$d(\sin\alpha + \sin\beta) = m\lambda, \tag{37}$$

and

$$\left(\frac{\cos^2\alpha}{r} - \frac{\cos\alpha}{R}\right) + \left(\frac{\cos^2\beta}{r'} - \frac{\cos\beta}{R}\right) = 0, \tag{38}$$

where d is the grating constant, α the angle of incidence at the grating, β the angle of diffraction, r the distance from the grating to the entrance slit, r' the distance from the grating to the focused image, and R

the radius of curvature of the grating. The signs of α and β are chosen so that they are different when the entrance slit and the image lie on opposite sides of the normal to the grating. Equation (37) is simply the interference relation which applies to any grating, Eq. (38) is the special focus condition for concave gratings. If each of the terms in parentheses of this equation are satisfied separately (Rowland circle conditions) then not only is the image in focus, but also many of the higher order aberrations are minimized. If the equation as a whole is satisfied, then it can only be said that the image is in focus.

If the angle between the entrance and exit slits is fixed with the value C, then this equation becomes,

$$\left(\frac{\cos^2\alpha}{r} - \frac{\cos\alpha}{R}\right) + \left(\frac{\cos^2(\alpha - c)}{r'} - \frac{\cos(\alpha - c)}{R}\right) = 0. \quad (39)$$

Now the only variables are α (which is determined by the desired output wavelength) and the distances from the slits to the grating. If r and α are chosen, then the equation is solved by,

$$\rho' = \cos\alpha(1 - \rho\cos\alpha)\sec^2(\alpha - C) + \sec(\alpha - C), \quad (40)$$

where $\rho = R/r$ and $\rho' = R/r'$. Values of ρ' which satisfy Eq. (40) guarantee good focus but promise nothing about the quality of the image. Solutions, as a function of α, of this equation are shown in Fig. 14, the parameter is ρ. Each of the curves in Fig. 14 may be considered the

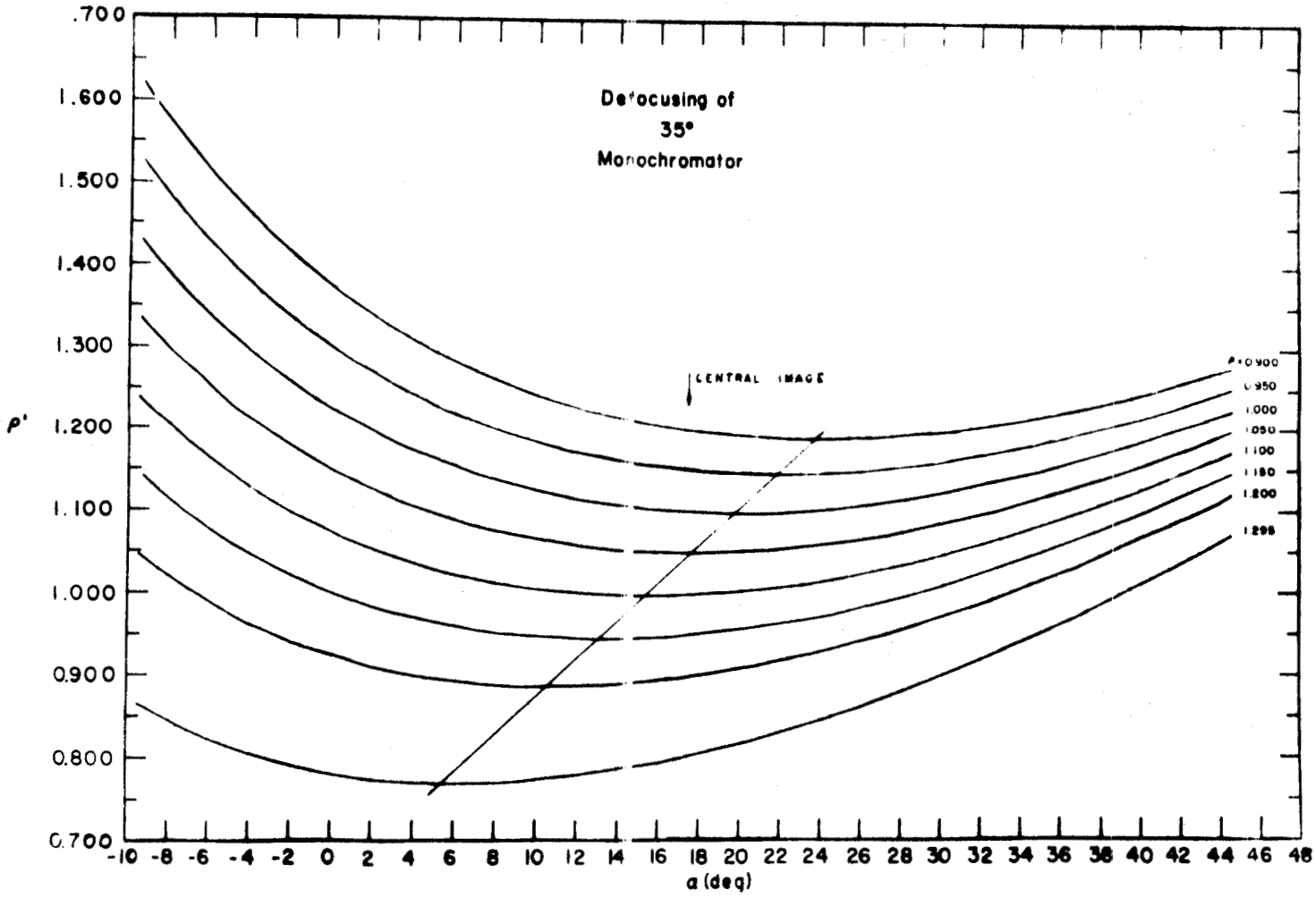

Fig. 14. Defocusing of the 35° Monochromator. The best focus is obtained by placing the exit slit near the minimum of the desired curve. The outside order is to the left of the central image in this figure and in Fig. 11.

defocusing characteristic of a particular geometry of the 35° monochromator. Each curve has a broad minimum at some value of α, or equivalently, at some wavelength, the exact value of which is determined by the number of grooves per unit length of the grating, Eq. (37). The monochromator can thus be designed to be in exact focus at two wavelengths, separated by an interval Δλ, say, and have a good focal range approximately equal to 2(Δλ). At this point the quality of the Seya geometry becomes obvious because the lower curve in Fig. 13 is shown on the same vertical scale as the parametric family in Fig. 14. The upper curve in Fig. 13, the reciprocal of the lower curve, is drawn with a 10x expanded scale.

For the present work, a 1440 groove/mm grating was available. The slit parameters were chosen so that for the first outside order, the angle of incidence at the grating of the undispersed radiation varied between 11.0° and 4.4° in the wavelength range between 1500 and 3000 Å, thus satisfying the normal incidence requirements. This placed the entrance slit 78.74 cm and the exit slit 124.6 cm from the grating. The focusing curve lies between the two lowest curves of Fig. 14.

For this arrangement, the focused image was always within 3 mm of the exit slit. No attempt was made to measure the maximum resolving power of the instrument,

but with the very wide slits mentioned in chapter III, the resolution was better than 3 Å in the design range $1500 < \lambda < 3000$ Å.** Qualitative experiments with narrower slits indicated that it could have been much better, probably less than one Angstrom unit, had the intensity transmitted by the sapphire reflectometer windows at shorter wavelengths permitted narrower slits. No calculations were made for the line profiles.

APPENDIX II

COMPUTER PROGRAMS

The following Fortran II programs were written for an IBM 1401 in order to produce the curves from which n and k were obtained (Fig. 5) and to expedite the reduction of the reflectance data. The 1401 is a binary coded decimal (BCD), variable instruction length machine having (in this case) 8000 core storage locations. Each of the individually addressable core spaces is capable of storing one digit, letter, or special character. Because of limited storage, the Fortran II software does not provide for arithmetic statement function, function subroutine, or subprogram programming.[70] Library functions include SINF, COSF, EXPF, LOGF, ABSF, XABSF, FLOATF, and XFIXF.[71]

The first program to be considered is listed in Table I: the associated flow diagram appears in Fig. 15. This program, which was used to calculate the curves shown in Fig. 5, computes the reflectance for a given n, k pair at a given angle of incidence. (The flow diagrams presented here were drawn to follow the associated Fortran programs as closely as possible. Simplicity, however,

```
SEQ   STMNT      FORTRAN STATEMENT                                    PAGE   1

      C              THIS PROGRAM COMPUTES THE REFLECTED INTENSITY AS A FUNCTION OF
      C            OPTICAL CONSTANTS, N AND K.  THE ANGLE OF INCIDENCE, PHI, IS A
      C            PARAMETER.  FOR THIS PROGRAM, N AND K ARE VARIED BETWEEN .01 AND
      C            1.0 IN STEPS OF 0.01.
  1    1000       READ 1, PHI, SINPHI, COSPHI, TANPHI, IPAGE
      C
  2       1        FORMAT ( F5.2, 3F7.5, I3)
  3               PRINT 2, PHI, IPAGE
  4       2       FORMAT (1H1, 10X, 6HPHI = ,F5.2,4H DEG, 96X, 4HPAGE, I4/ 60X,  12H
             1   REFLECTIVITY)
  5               CC = COSPHI*COSPHI
  6               SNTN = SINPHI*TANPHI
  7                 SNTN2 = SNTN*SNTN
  8               SS = SINPHI*SINPHI
  9               DIMENSION R(10)
 10               K = 0
 11               DO 100 N = 1, 100
 12               K = K + 1
 13               AN = FLOATF(N)*.01
 14               PRINT 3, AN
 15       3       FORMAT ( 11X, 4HN = , F 5.3/11X, 1HK, 9X, 1H0, 10X, 1H1, 10X, 1H2,
             1   10X, 1H3, 10X, 1H4, 10X, 1H5, 10X, 1H6, 10X, 1H7, 10X,1H8,10X,1H9)
 16               DO 200 M = 0, 9
 17               AMAR = FLOATF(M)* .1
 18               DO 300 L = 0, 9
 19               AK = AMAR + FLOATF(L)*.01
 20               J = L + 1
 21               Z = AN*AN - AK*AK - SS
```


Table I. Fortran Program for Calculation of Curves (see Fig. 5) from which the Optical Constants Corresponding to a Particular Experimental Reflectance Pair were Obtained.

Table I (Cont.)

```
SEQ    STMNT      FORTRAN STATEMENT                                    PAGE    2

 22               X = Z*Z
 23               Y = 2.*AN*AK
 24               Y =  Y*Y
 25               ASQBSQ = SQRTF(X + Y)
 26               IF (Z + ASQBSQ)  30,30,40
 27        30     X = 0.
 28               GO TO 41
 29        40     X = SQRTF((Z + ASQBSQ)*.5)
 30        41     CSPHX2 = 2.*COSPHI*X
 31               RS = (ASQBSQ + CC - CSPHX2)/(ASQBSQ + CC + CSPHX2)
 32       300     R(J) = RS*(ASQBSQ + SNTN2)/(ASQBSQ + SNTN2 + 2.*X*SNTN)
 33       200     PRINT 4, AMAR, R
 34         4     FORMAT (10X, F3.1,1X,10F11.5)
 35               IF(N -100) 50, 100, 60
 36        50     IF(K - 4) 80, 70, 60
 37        60     PRINT 5
 38         5     FORMAT (11X, 4(6HERROR ), 3HERR, 53(1H-), 3HZAP, 27(1H-)// 48X, 35
                1  HMESSAGE 007 - WHALLEY STRIKES AGAIN/1H1)
 39               STOP
 40        80     PRINT 6
 41         6     FORMAT (1H0/)
 42               GO TO 100
 43        70     IPAGE = IPAGE + 1
 44               PRINT 2, PHI, IPAGE
 45               K = 0
 46       100     CONTINUE
 47               GO TO 1000
 48               END
```

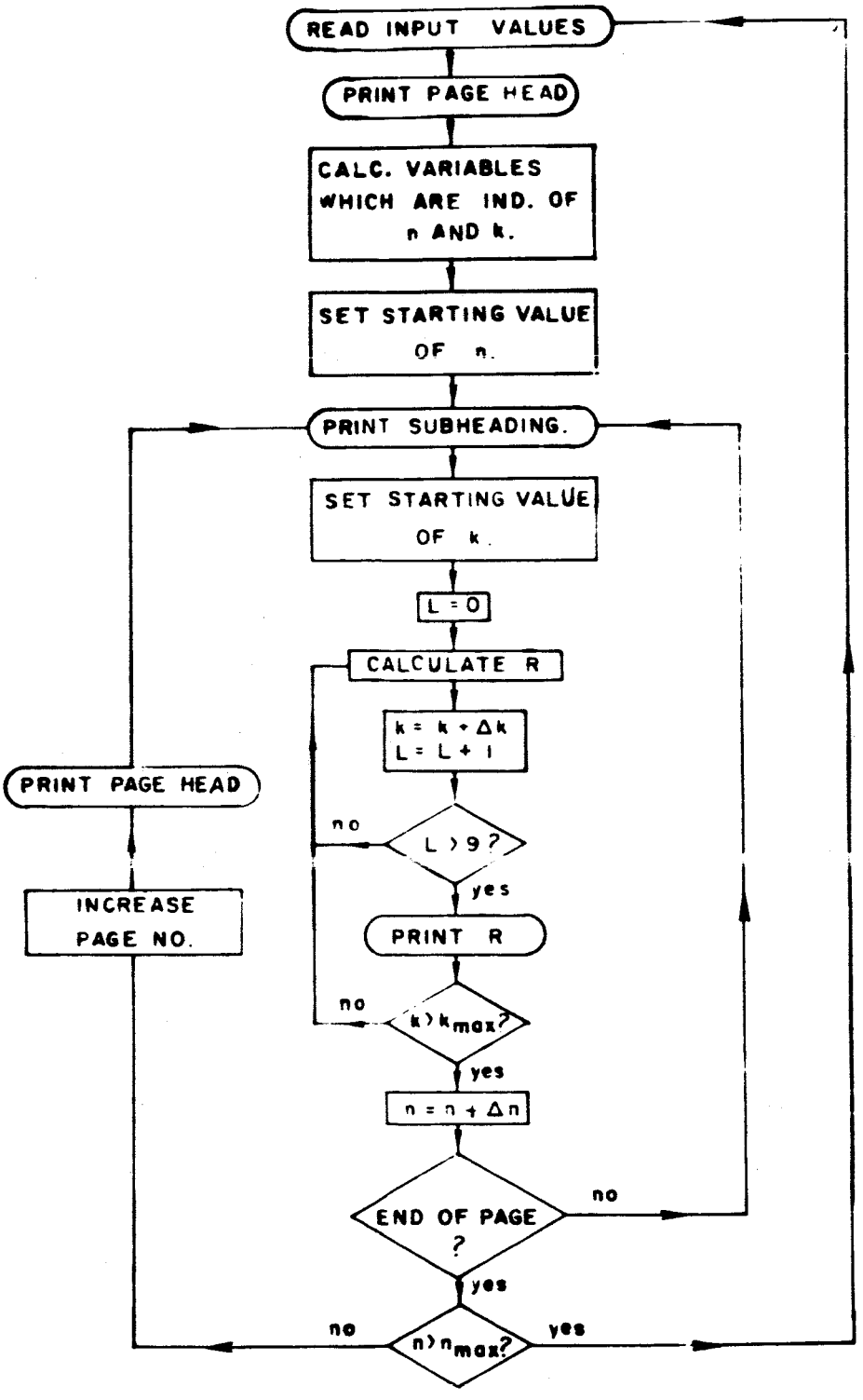

Fig. 15. Flow Diagram for Program Listed in Table I.

required that in the case of loops, the logical processes of the computer be followed rather than the more abstract language of the Fortran source program. The parenthetical numbers refer to sequence numbers in the program listing.)

The input data for this program (1) consists of one card which is punched with the angle of incidence, its sine, cosine, and tangent, and the page number for the first sheet of computer output. The trigonometric functions could, of course, have been computed by the machine, but the corresponding Fortran subroutine requires more than 400 core spaces, and in view of the limited storage of the 1401, the use of these subroutines would have been an extravagance which would have excluded more important parts of the program. This input data being accepted, the computer printed an informatory page heading (3,4) and then calculated (5-8) certain functions of the input data which were independent of n and k but which would be used repeatedly in the program. The starting value of the real part of the index of refraction is set by (13). A subheading was then printed (14,15) which identified the columns of numbers to appear later, and the starting value of k set (19). Since the calculated reflectances were to be printed in sets of ten, the variable L was invented to count the calculations and to inform the computer when it was time to

print an output line. The data were printed in blocks of 100 numbers (ten repetitions of the variable L through the range $0 \leq L < 10$) for which n was specified and k varied through a preset range (16,19). Therefore, after each line was printed, the computer checked to find out if the entire range of k had been covered. After each block of data (corresponding to one value of n) had been printed, the machine checked to see if it had come to the end of a page (36), if so, it added one to the page number and printed a new page heading, otherwise it simply printed a new subheading and continued the reflectance calculations. When the upper limit of n had been reached(46) the computer went to the start of the program and prepared to read new input data and calculate reflectances for a different angle of incidence.

The program used to convert the raw data into reflectances is listed in Table II, the flow diagram is given in Fig. 16, and the output is shown in Tables III and IV. The raw data, when taken from the charts, consist of a pair of numbers for each intensity measurement at a particular wavelength. One of these numbers represents the line height as measured on the chart, the other is an integer (fixed point number) which identifies the electrometer range applying to that particular measurement. At each wavelength of each run there were six

```
SEQ    STMNT      FORTRAN STATEMENT                                    PAGE    1

       C
       C              THIS PROGRAM TAKES THE EXPERIMENTAL INCIDENT AND REFLECTED
       C              INTENSITIES, NORMALIZES THEM, AND CALCULATES THE AVERAGE,
       C              THE ERROR, AND THE REFLECTIVITY FOR EACH ANGLE OF INCIDENCE.
       C
       C
       C              SCRATCH TAPES SHOULD BE MOUNTED ON TAPE UNITS 1 AND 2.
       C
  1                   DIMENSION   IHEAD(8), JHEAD(5), KHEAD(9), IDEP(3),
                 1               A(6), B(3), I(6), S(8), DATA(12)
       C
  2                   EQUIVALENCE  (AZ, A, DATA), (BZ, A(2)), (AG, A(3)), (BG, A(4)),
                 1                 (AN, A(5)), (BN, A(6)),
                 2                 (IHEAD(4), JHEAD), (IHEAD, IDEP, KHEAD), (KHEAD(9),
                 3                 LAMCNG),(KHEAD(8), NUMSER),
                 4                 (B, EV), (B(2), RG), (B(3), RN)
       C
  3     1000        READ 1, NUMLAM
  4                 DO 100 N = 1, NUMLAM
  5                 READ1, LAMBDA
  6       100       WRITE OUTPUT TAPE 1, 1, LAMBDA
  7                 END FILE 1
  8                 REWIND 1
  9                 J = NUMLAM/50
 10                 M = NUMLAM - 50*I
 11                 IF (M) 40, 40, 50
 12        40       M = 50
 13                 GO TO 51
 14        50       J = J + 1
```


Table II. Fortran Program to Convert Raw Data into Reflectance Pairs.

Table II (Cont.)

```
SEQ    STMNT      FORTRAN STATEMENT                                  PAGE    2

 15       51      READ 2
 16               READ 4, KHEAD
 17               READ 8, S
 18               IPAGE = -1
 19               DO 200 N = 1, J
 20               PRINT 3
 21               PRINT 2
 22               IF (IDEP) 10, 20, 10
 23       20      PRINT 5
 24               GO TO 30
 25       10      PRINT 6, IDEP
 26       30      PRINT 7, JHEAD, IPAGE
 27               PRINT 14
 28               IPAGE = IPAGE - 1
 29               MM = 50 - (N/J)*(50 - M)
 30               DO 300 NN = 1, MM
 31               READ 9, A, I
 32               DO 400 K = 1, 6
 33               I = I(K)
 34      400      A(K) = A(K) * S(I)
 35               RG = (AG + BG)/(AZ + BZ)
 36               RN = (AN + BN)/(AZ + BZ)
 37               DATA (10) = BN
 38               DATA (9) = AN
 39               DATA (6) = BG
 40               DATA (5) = AG
 41               DO 500 K = 3, 11, 4
 42               DATA(K) = (DATA(K-2) + DATA(K-1))/2.
```

Table II (Cont.)

```
SEQ    STMNT      FORTRAN STATEMENT                                    PAGE    3

 43      500      DATA(K+1) = ABSF(DATA(K) - DATA(K-1))/DATA(K)
 44               READ INPUT TAPE 1, 1, LAMBDA
 45               WRITE OUTPUT TAPE 2, 12, LAMBDA, RG, RN
 46      300      PRINT 11, LAMBDA, DATA, LAMBDA
 47      200      CONTINUE
 48               END FILE 2
 49               REWIND 2
 50               REWIND 1
 51               DO 600 N = 1, J
 52               PRINT 3
 53               PRINT 2
 54               IF (IDEP) 60, 70, 60
 55       70      PRINT 5
 56               GO TO 80
 57       60      PRINT 6, IDEP
 58       80      PRINT 7, JHEAD, IPAGE
 59               PRINT 13
 60               IPAGE = IPAGE - 1
 61               MM = 50 - (N/J)*(50 - M)
 62               DO 700 NN = 1, MM
 63               READ INPUT TAPE 2, 12, LAMBDA, RG, RN
 64               EV = 12394./ FLOATF(LAMBDA)
 65      700      PRINT 15, LAMBDA, B
 66      600      CONTINUE
 67               REWIND 2
 68               IF (LAMCNG) 1000, 51, 1000
      C
 69        1      FORMAT (I4)
```

Table II (Cont.)

```
SEQ    STMNT        FORTRAN STATEMENT                                    PAGE    4

 70        2          FORMAT (15X, 65H
     1                                                                  )
 71        3          FORMAT (1H1, 4(/))
 72        4          FORMAT (3I2/ 4I2, 2I4)
 73        5          FORMAT (/)
 74        6          FORMAT (15X, 18HFILM DEPOSITED ON , 2(I2, 1H/), I2)
 75        7          FORMAT (15X, 25HREFLECTIVITY MEASURED ON ,2(I2, 1H/), I2,
     1     10H.  RUN NO., I3, 48X, 8HSER. NO., I5, I3//)
 76        8          FORMAT (8F8.3)
 77        9          FORMAT (6F5.0, 6I1)
 78       11          FORMAT (I10, 3(1X, 3F10.0, F7.3), I7)
 79       12          FORMAT (I6, 2E20.8)
 80       13          FORMAT (/ 25X, 14HLAMBDA      EV, 10X, 2HRG, 8X, 2HRN, 10X,
     1     10HN         K  //)
 81       14          FORMAT (27X, 6HI-ZERO, 30X, 9HI-GRAZING, 30X, 8HI-NORMAL/
     1     11H     LAMBDA, 3(7H      1, 9X, 22H2      AVERAGE  ERROR ),
     2     7H LAMBDA)
 82       15          FORMAT (I30, F11.4, F12.4, F10.4)
 83                   END
```

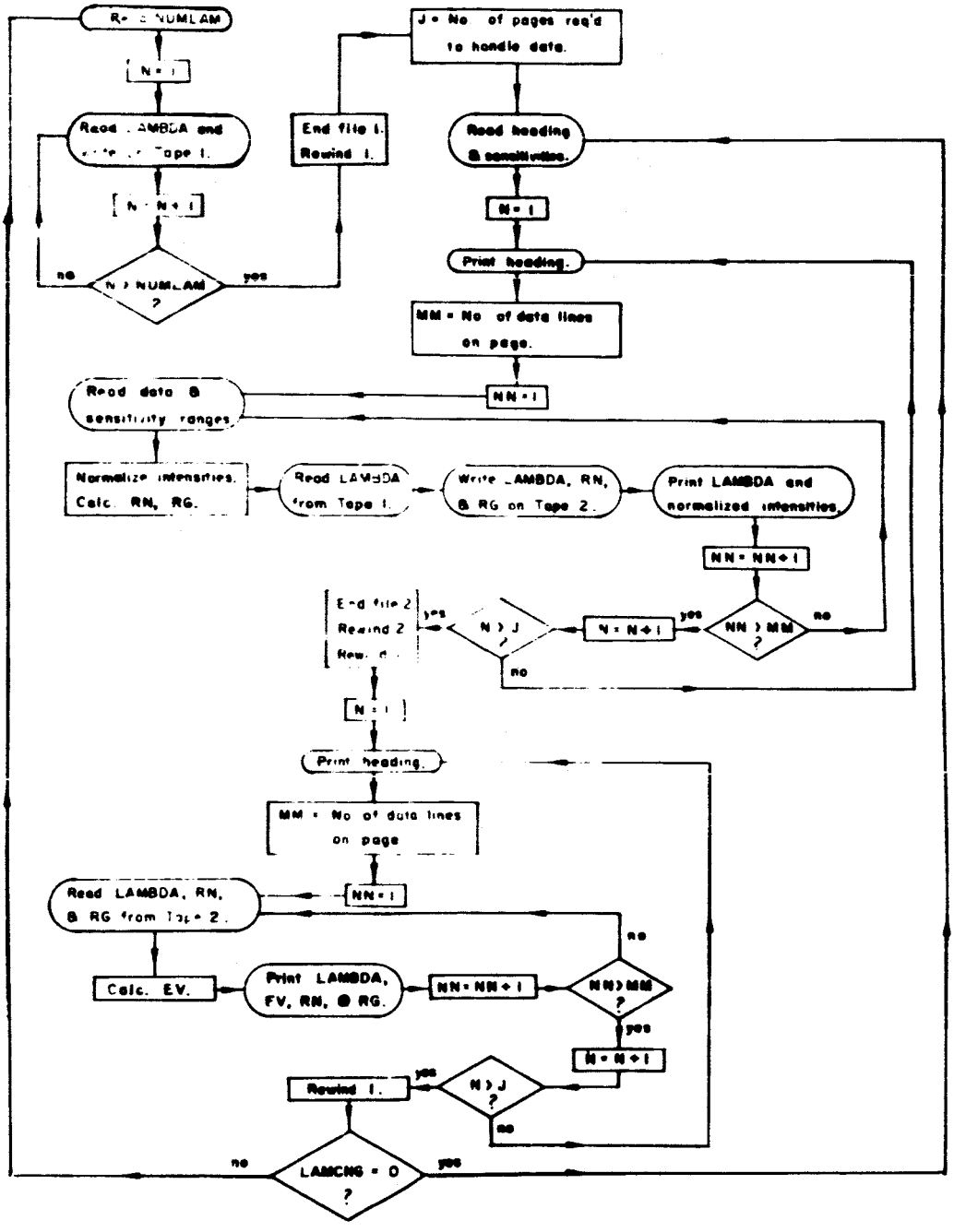

Fig. 16. Flow Diagram for Fortran Program Listed in Table II.

BARIUM ON CLEAN GLASS REF
FILM DEPOSITED ON 12/14/65
REFLECTIVITY MEASURED ON 12/14/65. RUN NO. 2 SAM. NO. 56-2

LAMBDA	I-ZERO 1	I-ZERO 2	I-ZERO AVERAGE	I-ZERO ERROR	I-GRATING 1	I-GRATING 2	I-GRATING AVERAGE	I-GRATING ERROR	I-NORMAL 1	I-NORMAL 2	I-NORMAL AVERAGE	I-NORMAL ERROR	LAMBDA
1455	324407.	317700.	321054.	0.010	209270.	204740.	206505.	0.009	9074.	9493.	9283.	0.023	1455
1468	250030.	243217.	247124.	0.015	159203.	159203.	159203.	0.000	7957.	8027.	7992.	0.004	1468
1480	559911.	543208.	556530.	0.015	163141.	164449.	166234.	0.001	20661.	20475.	20818.	0.008	1480
1489	544749.	533384.	542087.	0.005	159707.	159707.	159707.	0.000	20591.	21359.	20975.	0.018	1489
1498	355224.	342410.	348817.	0.018	231584.	228131.	229980.	0.007	12564.	13471.	13018.	0.035	1498
1511	858819.	831910.	845365.	0.015	560211.	558505.	559858.	0.001	47555.	47211.	47441.	0.004	1511
1520	774345.	757017.	765681.	0.011	504555.	503711.	505143.	0.003	46536.	45172.	46384.	0.005	1520
1542	1201047.	1168557.	1184802.	0.014	743181.	736355.	790074.	0.001	78883.	76354.	76619.	0.003	1542
1578	2473751.	2500647.	2487220.	0.005	1430561.	1492724.	1631844.	0.001	134597.	134432.	135015.	0.003	1578
1589	2270881.	2285130.	2277551.	0.003	1548630.	1544358.	1546524.	0.001	147773.	187761.	187867.	0.001	1589
1608	5374464.	5458440.	5416452.	0.018	3500934.	3705441.	3405720.	0.028	467140.	461432.	484319.	0.004	1608
1621	2079340.	1595949.	2037465.	0.020	1351564.	1345088.	1348345.	0.002	192163.	190078.	190081.	0.011	1621
1640	1878039.	1812942.	1844491.	0.017	1220541.	1214043.	1217232.	0.003	180384.	185431.	183007.	0.003	1640
1672	513615.	497730.	505513.	0.016	334291.	332171.	333232.	0.003	57714.	57716.	57715.	0.000	1672
1700	276359.	262279.	269339.	0.025	182854.	174029.	178442.	0.025	33885.	35477.	34682.	0.023	1700
1750	230842.	225920.	228391.	0.011	149672.	144495.	148384.	0.011	33974.	34150.	34047.	0.002	1750
1800	232980.	223802.	228391.	0.020	148260.	147554.	147907.	0.002	37535.	37484.	37542.	0.001	1800
1850	252395.	240040.	246218.	0.025	157741.	154967.	156374.	0.009	44207.	43737.	43472.	0.006	1850
1900	265103.	256396.	261750.	0.013	166263.	142733.	164438.	0.011	48714.	49667.	47141.	0.010	1900
1950	271910.	261220.	266515.	0.020	168381.	165310.	167165.	0.007	52844.	53056.	52950.	0.002	1950
2000	303560.	293343.	298462.	0.017	185678.	185678.	185678.	0.000	50575.	40787.	40681.	0.002	2000
2050	410852.	395360.	403126.	0.019	250983.	252395.	251689.	0.003	52708.	63974.	63341.	0.008	2050
2100	638930.	607160.	623045.	0.025	377004.	381240.	379122.	0.004	128774.	131528.	130151.	0.011	2100
2150	509720.	863151.	886436.	0.026	536713.	536560.	536737.	0.000	635400.	647167.	642204.	0.011	2150
2200	1110075.	1079751.	1094913.	0.014	667170.	669288.	668229.	0.002	247150.	244275.	245583.	0.006	2200
2250	1277940.	1234620.	1256280.	0.017	751537.	744477.	748007.	0.005	263137.	282430.	285754.	0.012	2250
2300	1391655.	1355516.	1373766.	0.013	801420.	807918.	804669.	0.004	321230.	316208.	318759.	0.006	2300
2350	1475046.	1518366.	1496706.	0.014	867483.	866400.	866942.	0.001	356177.	349823.	353000.	0.009	2350
2400	1700310.	1650492.	1675401.	0.015	964953.	966036.	965495.	0.001	403126.	393516.	401361.	0.004	2400
2450	1960230.	1509329.	1934780.	0.013	1097079.	1095996.	1096538.	0.000	466313.	464901.	465607.	0.002	2450
2500	2170332.	2103186.	2136759.	0.016	1202130.	1201047.	1201569.	0.000	522087.	516557.	523322.	0.003	2500
2600	1883337.	1823772.	1853555.	0.016	1023435.	1023435.	1023435.	0.000	456547.	453605.	455076.	0.003	2600
2700	1778286.	1825938.	1802112.	0.013	984447.	963364.	983905.	0.001	447957.	446545.	447251.	0.002	2700
2800	1808610.	1751211.	1779911.	0.016	968202.	963870.	966035.	0.002	451134.	449722.	450428.	0.002	2800
2900	1678650.	1624500.	1651575.	0.016	892392.	890226.	891309.	0.001	428542.	425718.	427130.	0.003	2900
3000	1475046.	1440390.	1457718.	0.012	788424.	781926.	785175.	0.004	384770.	381945.	383358.	0.004	3000
3100	1353750.	1322343.	1338047.	0.012	727776.	723444.	725610.	0.003	363943.	363943.	363943.	0.000	3100

74

Table III. First Page of Output of Program of Table II. The wavelength for each data point is given along with the normalized intensities, the average, and the precision for each of the pairs of I_o, I_g, and I_n.

BARIUM ON CLEAN GLASS HCL
FILM DEPOSITED ON 12/14/69
REFLECTIVITY MEASURED ON 12/14/69. RUN NO. 2

LAMBDA	EV	RG	RN	N	K
1455	8.5182	0.6432	C.0289		
1460	8.4928	0.6447	C.0324		
1480	8.3763	0.6569	0.0375		
1489	8.3237	0.6636	C.0387		
1498	8.2737	0.6693	0.0373		
1511	8.2025	0.6618	C.0961		
1528	8.1113	0.6597	C.0606		
1542	8.0376	0.6702	0.0647		
1576	7.8642	0.6801	C.0784		
1584	7.7599	0.6789	0.0825		
1608	7.7077	0.6657	C.0894		
1621	7.6454	C.6617	0.0933		
1640	7.5573	0.6598	C.1CC8		
1672	7.4127	0.6590	C.1141		
1700	7.2906	0.6625	0.1288		
1750	7.0823	0.6484	C.1491		
18CC	6.8854	0.6476	C.1644		
1850	6.6999	0.6391	C.1766		
1900	6.5232	0.6285	0.1879		
1950	6.3559	0.6272	C.1987		
2000	6.1970	0.6221	C.2033		
2050	6.0459	0.6243	C.2087		
2100	5.9019	0.6085	C.2089		
2150	5.7647	0.6055	C.7246		
2200	5.6336	0.6103	C.2244		
2250	5.5084	0.5954	C.2275		
2300	5.3887	0.5857	C.2320		
2350	5.2740	0.5792	C.2359		
2400	5.1642	0.5763	C.2396		
2450	5.0588	0.5668	C.2407		
2500	4.9576	0.5623	0.2435		
2600	4.7669	0.5521	C.2461		
2700	4.5904	0.5460	C.2482		
2800	4.4264	0.5427	C.2531		
2900	4.2738	0.5397	C.2586		
3000	4.1313	0.5386	C.2630		
3100	3.9981	0.5423	C.2720		

Table IV. Second Page of Output of Program of Table II. The wavelength, photon energy (in eV), and reflectances are tabulated. Two blank columns are to be filled in manually when the optical constants are obtained from the charts.

such pairs of numbers--two each for I_o, I_n, and I_g. For each data point, one card was punched with these numbers. The program normalized the data (i.e., multiplied the data by the relative electrometer sensitivity and hence converted all the intensities to a common scale), averaged it, and calculated the precision at each wavelength. This information was printed along with the corresponding wavelength (Table III). The computer then calculated and printed the reflectance pair R_n and R_g, and, for convenience, the photon energy (Table IV).

The program was written so that the number of datum points could be changed from time to time. Therefore, starting now in the upper left hand corner of Fig. 16 (in which variable names are written with capital letters), the first operation is to read the number of datum points to be considered for the ensuing run. Having learned the number of datum points (NUMLAM), the computer then reads the corresponding wavelengths from the next NUMLAM cards and writes them as successive records on magnetic tape (3-8). Since the number of datum points is variable, it is then necessary for the machine the calculate (9-14) the number of pages required to represent the data in the printed output. Heading information is then read from the next three cards (15, 16) which include comments on the run (15),

the date of evaporation of the film (16), the date of the measurement, and a serial and run number which was assigned to each data set (16). The relative electrometer sensitivities are obtained from the next card (17) and a page numbering sequence which labels the number of pages for the particular data set is started (18). The variable IPAGE exists only for the convenience of those using the results of the computation. The program does not at any time branch on this variable and it should not be confused with N (19) which is the loop index. The test value J for this loop determines the number of pages in the output.

The information obtained in sequence (15, 16) is printed (20-26) along with Hollerith constants (27, 81) which provide the column headings (see Table III). The number of lines (29) for the page is calculated. Here either MM = 50 or MM = NUMLAM - 50 x (some integer), i.e., the total number of datum points (NUMLAM) minus some multiple of 50. The latter alternative always results in a value less than 50 for MM. (In other words, for 109 datum points, MM = 50 for the first two pages and MM = 9 for the third and last page.) The line counting DO index, NN, is established by (30). The next NUMLAM cards now contain the raw data. The intensities A and the corresponding electrometer ranges I are read (31)

(each of the variables A, I are actually six-element arrays), and the raw intensities replaced in storage by their normalized values (32-34). The reflectivities are calculated (35, 36) and the normalized intensities inserted in their proper positions in the output array DATA (37-40) for later printing (46). The average and precision for the intensity pairs are calculated in (41-43). The corresponding wavelength is obtained from Tape 1 (44), the wavelength and reflectances are written on Tape 2 for later reference (45), and the results of the normalization and averaging processes printed (46) in the format shown in Table III. This process is continued, printing new page headings when necessary, until all of the input data has been processed.

The computer is now finished processing the data, but has not been able to display it because the printer forms are not wide enough to include the reflectances along with the other information in Table III. This information must now be retrieved from Tape 2 and printed.

The page headings which had been used on the preceeding pages are printed again (52-59) and the line counting calculations repeated (61). The wavelength and reflectances are read from Tape 2 (63), the photon energy calculated in eV (64), and the result printed as shown in Table IV. If any number other than zero has been

punched in any of cols. 13 - 16 of the third card of the data set (the card which also includes the date of measurement, the serial number, and the run number), then the value of LAMCNG is different from zero and the program prepares to read a new set of wavelengths. If LAMCNG = 0, it branches back to (15) and continues processing a new set of data cards, but using the original set of wavelengths written on Tape 1. It was easy to add this option to the program but its use is somewhat ponderous because the LAMCNG signal must be punched in the heading cards of the set preceeding that to which it applies.

After the blank columns in Table IV had been filled in manually by reading n and k from charts similar to that shown in Fig. 5, a second deck of cards having the same heading cards as the deck containing the raw data was punched. This deck was used in conjunction with the program listed in Table V to calculate the components of the complex dielectric constant and the energy loss functions $\mathrm{Im}(1/\varepsilon)$ and $\mathrm{Im}[1/(\varepsilon + 1)]$. No flow diagram or explanation for this program is given because it is logically very similar to that of Fig. 14. The program is shorter because the printed output is simpler and does not require the intermediate use of magnetic tape.

The rather complicated EQUIVALENCE and DIMENSION statements of these last two programs were necessary in

```
SEQ   STMNT      FORTRAN STATEMENT                                    PAGE   1

      C
      C              THIS PROGRAM COMPUTES IM(1/E), IM(1/E+1), AND THE REAL AND
      C              IMAGINARY PARTS OF THE COMPLEX DIELECTRIC CONSTANT FROM N AND K
      C              (THE OPTICAL CONSTANTS).
      C
      C              A SCRATCH TAPE SHOULD BE MOUNTED ON TAPE UNIT 1.
      C
    1                 DIMENSION KHEAD(9), JHEAD(5), IDEP(3),
                     1            DATA(7)
      C
    2                 EQUIVALENCE  (KHEAD,IDEP), (KHEAD(4), JHEAD), (KHEAD(9), LAMCNG),
                     1             (DATA, EV), (DATA(2), AN), (DATA(3), AK),
                     2             (DATA(4), E1), (DATA(5), E2), (DATA(6), FAKE1),
                     3             (DATA(7), FAKE2)
      C
    3     1000       READ 1, NUMLAM
    4                DO 100 N = 1, NUMLAM
    5                READ 1, LAMBDA
    6      100       WRITE OUTPUT TAPE 1, 1, LAMBDA
    7                END FILE 1
    8                REWIND 1
    9                I = NUMLAM/50
   10                M = NUMLAM - 50*I
   11                IF (M) 40, 40, 50
   12       40       M = 50
   13                GO TO 51
   14       50       I = I + 1
   15       51       IPAGE = -2*I  - 1
```


Table V. Fortran Program Used to Calculate the Complex Dielectric Constant and Energy Loss Functions from the Optical Constants.

Table V (Cont.)

```
SEQ    STMNT      FORTRAN STATEMENT                                  PAGE    2

 16               READ 2
 17               READ 4, KHEAD
 18               DO 200 N = 1, I
 19               PRINT 3
 20               PRINT 2
 21               IF (IDEP) 10, 20, 10
 22         20    PRINT 5
 23               GO TO 30
 24         10    PRINT 6, IDEP
 25         30    PRINT 7, JHEAD, IPAGE
 26               PRINT 8
 27               IPAGE = IPAGE - 1
 28               MM = 50 - (N/I)*(50 - M)
 29               IF (MM) 60, 200, 60
 30         60    DO 300 NN = 1, MM
 31               READ 9, AN, AK
 32               READ INPUT TAPE 1, 1, LAMBDA
 33               EV = 12394./FLOATF(LAMBDA)
 34               AA = AN*AN
 35               BB = AK*AK
 36               E1 = AA - BB
 37               E2 = 2.*AN*AK
 38               G = AA - BB + 1.
 39               FAKE1 = E2/(AA+ BB)/(AA + BB)
 40               FAKE 2 = E2/(G*G + 4.*AA*BB)
 41        300    PRINT 11, LAMBDA, DATA
 42        200    CONTINUE
 43               REWIND 1
```

Table V (Cont.)

```
SEQ    STMNT        FORTRAN STATEMENT                                    PAGE    3

 44                  IF (LAMCNG) 1000, 51, 1000
 45         1        FORMAT (I4)
 46         2        FORMAT (15X, 65H
           1
 47         3        FORMAT (1H1, 4(/))
 48         4        FORMAT (3I2/4I2, 2I4)
 49         5        FORMAT (/)
 50         6        FORMAT (15X, 18HFILM DEPOSITED ON , 2(I2,1H/), I2)
 51         7        FORMAT (15X, 25HREFLECTIVITY MEASURED ON , 2(I2,1H/), I2,
           1    10H.  RUN NO., I3, 48X, 8HSER. NO. , I5, I3//)
 52         8        FORMAT (14X, 6HLAMBDA, 6X, 2HEV, 9X, 1HN, 9X, 1HK, 10X, 2HE1, 12X,
           1    2HE2, 10X, 7HIM(1/E), 6X, 9HIM(1/E+1))
 53         9        FORMAT (2F5.3)
 54        11        FORMAT (I19, F11.4, 2F10.3, 1P4E14.3)
 55                  END
```

order to arrange certain of the stored variables in consecutive storage locations in the computer. Thus the numbers occupying certain addresses could be treated as individual variables at one time and as parts of an array at other times. The main advantage of this occurred in some of the input/output lists -- (16, 25, 26, and 46) of Table II--which would have taken up much more storage space if the variables had been named separately.

BARIUM ON GLASS SUBSTRATE, KCL.
FILM DEPOSITED ON 12/14/69
REFLECTIVITY MEASURED ON 12/14/69. RUN NO. 2

LAMBDA	EV	N	K	E1	E2	IM(1/E)	IM(1/(E+1))
1455	8.5182	0.737	0.129	5.265E-01	1.901E-01	6.067E-01	[illegible]
1468	8.4428	0.725	0.140	5.040E-01	2.030E-01	6.829E-01	[illegible]
1480	8.3743	0.707	0.147	4.782E-01	2.079E-01	7.644E-01	[illegible]
1489	8.3237	0.701	0.147	4.698E-01	2.061E-01	7.831E-01	[illegible]
1498	8.2737	0.702	0.149	4.706E-01	2.092E-01	7.887E-01	3.451E-02
1511	8.2025	0.658	0.190	3.969E-01	2.500E-01	1.136E 00	1.242E-01
1528	8.1113	0.650	0.202	3.817E-01	2.626E-01	1.223E 00	1.328E-01
1542	8.0376	0.638	0.203	3.658E-01	2.590E-01	1.289E 00	1.340E-01
1578	7.8542	0.615	0.235	3.230E-01	2.891E-01	1.538E 00	1.577E-01
1598	7.7599	0.605	0.244	3.113E-01	2.972E-01	1.604E 00	1.644E-01
1608	7.7077	0.599	0.253	2.917E-01	3.103E-01	1.711E 00	1.756E-01
1621	7.6459	0.595	0.270	2.411E-01	3.213E-01	1.763E 00	1.842E-01
1640	7.5573	0.586	0.286	2.705E-01	3.375E-01	1.857E 00	1.932E-01
1672	7.4127	0.570	0.316	2.250E-01	3.602E-01	1.997E 00	2.209E-01
1700	7.2906	0.533	0.341	1.578E-01	3.635E-01	2.248E 00	2.430E-01
1750	7.0823	0.545	0.405	1.330E-01	4.415E-01	2.077E 00	2.785E-01
1800	6.8856	0.540	0.450	8.910E-02	4.870E-01	1.991E 00	3.417E-01
1850	6.6595	0.540	0.490	5.150E-02	5.292E-01	1.872E 00	3.817E-01
1900	6.5232	0.543	0.532	1.184E-02	5.778E-01	1.730E 00	[illegible]
1950	6.3559	0.541	0.562	-2.316E-02	6.081E-01	1.642E 00	[illegible]
2000	6.1970	0.547	0.586	-4.419E-02	6.411E-01	1.552E 00	4.840E-01
2050	6.0459	0.552	0.612	-6.984E-02	6.756E-01	1.454E 00	5.112E-01
2100	5.9019	0.567	0.633	-7.920E-02	7.178E-01	1.376E 00	5.256E-01
2150	5.7647	0.572	0.670	-1.217E-01	7.665E-01	1.273E 00	5.541E-01
2200	5.6336	0.582	0.700	-1.513E-01	8.148E-01	1.186E 00	5.886E-01
2250	5.5084	0.592	0.722	-1.708E-01	8.548E-01	1.125E 00	6.027E-01
2300	5.3887	0.613	0.764	-2.079E-01	9.367E-01	1.017E 00	6.225E-01
2350	5.2740	0.630	0.796	-2.367E-01	1.003E 00	9.444E-01	6.314E-01
2400	5.1642	0.639	0.817	-2.572E-01	1.044E 00	9.022E-01	6.370E-01
2450	5.0588	0.663	0.848	-2.795E-01	1.124E 00	8.376E-01	6.305E-01
2500	4.9576	0.678	0.872	-3.007E-01	1.182E 00	7.943E-01	6.256E-01
2600	4.7669	0.709	0.914	-3.327E-01	1.296E 00	7.239E-01	6.099E-01
2700	4.5904	0.730	0.942	-3.545E-01	1.375E 00	6.918E-01	5.958E-01
2800	4.4264	0.748	0.972	-3.853E-01	1.454E 00	6.426E-01	5.834E-01
2900	4.2738	0.765	1.004	-4.228E-01	1.536E 00	6.051E-01	5.704E-01
3000	4.1313	0.776	1.026	-4.505E-01	1.592E 00	5.815E-01	5.612E-01
3100	3.9981	0.775	1.050	-5.019E-01	1.728E 00	5.611E-01	5.718E-01

Table VI. Output of Program Listed in Table V. From left to right the columns are: wavelength, photon energy, n, k, $\varepsilon_1, \varepsilon_2$, $Im(1/\varepsilon)$, and $Im[1/(\varepsilon + 1)]$.

REFERENCES

*The numerator (e.g.) on the left side of Eq. (34) is the total signal (above the KCl background) at λ_1, the numerator on the right hand side is the pure light with $\lambda = \lambda_1$, a quantity which is never actually measured. In calculating the reflectances, no attempt was made to correct for the small error in I_o caused by a scattered light having wavelength shorter than 1750 Å.

**Very similar calculations have been carried out by R. I. Schoen (Boeing Scientific Research Laboratories, Seattle, Washington, unpublished), for a grazing incidence monochromator in which the angle between the entrance and exit arms was 140°. His requirement was that the monochromator be in focus at 200 and 400 Å. He found that this condition was satisfied for a 600 groove/mm, one meter grating with r = 31.898302 cm, and r' = 36.5210 cm. For this case the monochromator provided good focus (focused image within 0.38 of the exit slit) from 160 to 440 Å. His wavelength range is much narrower than for the present monochromator because of the grazing incidence design and because his focus requirements were about ten times more stringent than ours (.38 mm compared with 3.0 mm). For more dispersive gratings the defocusing

was much worse because of the larger grating rotation required to scan the same wavelength range.

[1]"First International Conference on Vacuum Ultraviolet Radiation Physics," Conference Proceedings, J. Quant. Spectrosc. Radiat. Transfer 2, 315-728 (1962).

[2]R. Tousey, J. Opt. Soc. Am. 51, 384 (1961).

[3]T. Violett and W. A. Rense, Astrophys. J. 130, 954 (1959).

[4]G. L. Weissler, Handbuch der Physik, XXI, 303 (1956).

[5]R. W. Roberts and T. A. Vanderslice, Ultrahigh Vacuum and its Applications (Prentice-Hall, Inc., Englewood Cliffs, New Jersey, 1963).

[6]J. L. Robins and P. E. Best, Proc. Phys. Soc. (London) 79, 110 (1962).

[7]M. Parker Givens, Solid State Physics 6, 313 (1958).

[8]M. Born and E. Wolf, Principles of Optics (Pergamon Press, London, 1959); A. C. Hall, J. Opt. Soc. Am. 55, 911 (1965).

[9]A. I. Mahan, J. Opt. Soc. Am. 46, 913 (1956).

[10]A. Kundt, Ann. Physik 34, 469 (1888).

[11]P. Drude, Ann. Physik 32, 584 (1887); 34, 489 (1888); 39, 481 (1890); 64, 159 (1898).

[12]P. Drude, The Theory of Optics (Dover Publications, Inc., New York, 1959).

[13]F. A. Jenkins and H. E. White, Fundamentals of Optics (McGraw-Hill Book Co., Inc., New York, 1950).

[14]W. R. Hunter, J. Opt. Soc. Am. 55, 1197 (1965).

[15]R. N. Hamm, R. A. MacRae, and E. T. Arakawa, J. Opt. Soc. Am. 55, 1460 (1965).

[16]R. Tousey, J. Opt. Soc. Am. 29, 235 (1939); C. Boeckner, J. Opt. Soc. Am. 19, 7 (1929); J. R. Collins and R. O. Bock, Rev. Sci. Instr. 14, 135 (1943); I. Simon, J. Opt. Soc. Am. 41, 336 (1951); K. Ishiguro, T. Sasaki, and S. Nomura, Sci. Papers Coll. Gen. Educ. Univ. Tokyo 10, 207 (1960); K. Ishiguro and T. Sasaki, Sci. Papers Coll. Gen. Educ. Univ. Tokyo 12, 19 (1962).

[17]R. H. Huebner, E. T. Arakawa, R. N. Hamm and R. A. MacRae, J. Opt. Soc. Am. 54, 1434 (1964).

[18]J. M. Bennett and M. J. Booty, Appl. Opt. 5, 41 (1966).

[19]S. P. F. Humphreys-Owen, Proc. Phys. Soc. (London) 77, 949 (1952).

[20]W. C. Johnson, Rev. Sci. Instr. 35, 1375 (1964); W. C. Walker, Appl. Opt. 3, 1457 (1964).

[21]D. G. Avery, Proc. Phys. Soc. (London) 65, 425 (1951).

[22]J. R. MacDonald and M. K. Brachman, Rev. Mod. Phys. 28, 393 (1956).

[23]H. Bode, Network Analysis and Feedback Amplifier Design (D. Van Nostrand Co., Inc., New York, 1945).

[24]F. Stern, Solid State Phys. 15, 299 (1963); C. Kittel, Elementary Statistical Physics (John Wiley and Sons, Inc., New York, 1958).

[25]B. Andermann, A. Caron, and D. Dows, J. Opt. Soc. Am. 55, 1210 (1965); F. C. Jahoda, Phys. Rev. 107, 1261 (1957); D. G. Thomas and J. Hopfield, Phys. Rev. 116, 573 (1959); M. Gottlieb, J. Opt. Soc. Am. 50, 343 (1960); O. P. Rustgi, J. S. Nodvik, and G. L. Weissler, Phys. Rev. 122, 1131 (1961); M. P. Rimmer and D. L. Dexter, J. Appl. Phys. 31, 775 (1960).

[26]H. E. Bennett and W. F. Koehler, J. Opt. Soc. Am. 50, 1 (1960).

[27]L. Marton, L. B. Leder, and H. Mendlowitz, Advances in Electronics and Electron Physics (Academic Press, Inc., New York, 1955) 7, 183; L. Marton, Rev. Mod. Phys. 28, 172 (1956).

[28]H. Mendlowitz, Proc. Phys. Soc. (London) 75, 664 (1960).

[29]D. Pines, Rev. Mod. Phys. 28, 184 (1956).

[30]L. B. Leder, Phys. Rev. 103, 1721 (1956).

[31]L. B. Leder, H. Mendlowitz, and L. Marton, Phys. Rev. 101, 1460 (1955).

[32]P. Lenard, Ann. Phys. 56, 255 (1895).

[33]G. E. Leithaüser, Ann. Phys. 15, 283 (1904).

[34]J. A. Becker, Phys. Rev. 23, 664 (1924).

[35]G. Ruthemann, Naturwissenschaften 29, 648 (1941); 30, 145 (1942); Ann. Phys. (6) 2, 113 (1948).

[36]C. J. Powell and J. B. Swan, Phys. Rev. 115, 869 (1959); 116, 81 (1959); 118, 640 (1960).

[37]L. Marton and L. B. Leder, Phys. Rev. 94, 203 (1954); 95, 1345 (1854); H. Watanabe, J. Phys. Soc. Japan 9, 920 (1954); 9, 1035 (1954); Phys. Rev. 95, 1684 (1954); D. Gabor and G. W. Jull, Nature 175, 718 (1955).

[38]D. Bohm and D. Pines, Phys. Rev. 82, 625 (1951); 85, 338 (1952); 92, 608 (1953); D. Pines, Phys. Rev. 92, 626 (1953).

[39]R. A. Ferrell, Phys. Rev. 111, 1214 (1948).

[40]W. Steinmann, Phys. Rev. Letters 5, 470 (1960); Z. Physik 163, 92 (1961).

[41]R. W. Brown, P. Wessel, and E. P. Trounson, Phys. Rev. Letters 5, 472 (1960).

[42]V. P. Silin and E. P. Fetisov, Phys. Rev. Letters 7, 374 (1961); E. A. Stern, Phys. Rev. Letters 8, 7 (1962).

[43]R. H. Ritchie and H. B. Eldridge, Phys. Rev. 126, 1935 (1962).

[44]I. M. Frank and V. I. Ginsburg, J. Phys. (USSR) 9, 353 (1945).

[45]H. Fröhlich and H. Pelzer, Proc. Phys. Soc. (London) A68, 525 (1955).

[46]L. Marton, J. Quant. Spectrosc. Radiat. Transfer 2, 671 (1962).

[47]R. E. LaVilla and J. Mendlowitz, Appl. Opt. 4, 955 (1965).

[48]H. Mendlowitz, J. Opt. Soc. Am. 50, 739 (1960).

[49]R. H. Ritchie, Phys. Rev. 106, 874 (1957).

[50]E. A. Stern and R. A. Ferrell, Phys. Rev. 120, 130 (1960).

[51]M. D. Wagner, L. Marton, and J. A. Simpson, Bull. Am. Phys. Soc. 5, 68 (1960).

[52]H. Kanazawa, Prog. Theoret. Phys. (Kyoto) 26, 851 (1961).

[53]T. Sasaki, J. Phys. Soc. Japan 18, 701 (1963).

[54]S. Yamaguchi, J. Phys. Soc. Japan 18, 266 (1963).

[55]R. P. Madden, Physics of Thin Films (Academic Press, New York, 1963), Vol. 1, p. 123.

[56]L. Elsworth and L. Holland, Brit. J. Appl. Phys. 14, 593 (1963).

[57]Purchased from Consolidated Vacuum Corporation, 1775 Mt. Read Blvd., Rochester, New York.

[58]T. Batzer and R. Ullman, Engineering Note, Lawrence Radiation Lab., Univ. of California, May 24, 1960 and October 7, 1960.

[59]W. Steinmann, E. I. Fisher, and G. L. Weissler, Optical Constants of Metals in the Vacuum Ultraviolet Region (Tech. Rept. prepared for NASA, January 15, 1964).

[60]F. Masuda and M. Seya, Sci. Light (Tokyo) 12, 9 (1963).

[61]H. M. O'Bryan, J. Opt. Soc. Am. 26, 122 (1936).

[62]R. J. Maurer, Phys. Rev. 57, 653 (1940).

[63]R. S. Minor, Ann. Phys. 10, 614 (1903); G. Joos and A. Klopfer, Z. Physik 138, 251 (1954); M. Priol, M. Lavor, and S. Robin, C. R. Acad. Sci. (France) 259, 3983 (1964); R. H. Huebner, E. T. Arakawa, R. N. Hamm, and R. A. MacRae, J. Opt. Soc. Am. 54, 1434 (1964); L. R. Canfield and G. Hass, J. Opt. Soc. Am. 55, 61 (1965).

[64]E. Rudberg, Phys. Rev. 50, 138 (1936).

[65]R. Tousey, Appl. Opt. 1, 679 (1962).

[66]H. G. Beutler, J. Opt. Soc. Am. 35, 311 (1945).

[67]T. Namioka, J. Opt. Soc. Am. 49, 446 (1959).

[68]M. Seya, Sci. Light (Tokyo) 2, 8 (1952).

[69]K. Rabinovitch, L. R. Canfield, and R. P. Madden, Appl. Opt. 4, 1005 (1965).

[70]D. D. McCracken, A Guide to Fortran Programming (John Wiley and Sons, Inc., New York, 1964).

[71]IBM 1401 Program Library, 1401 FORTRAN SYSTEM, 1401-FO-050 (1962).

UNCLASSIFIED

Security Classification

DOCUMENT CONTROL DATA - R&D

(Security classification of title, body of abstract and indexing annotation must be entered when the overall report is classified)

1. ORIGINATING ACTIVITY (Corporate author) Department of Physics University of Southern California Los Angeles, California 90007	2a. REPORT SECURITY CLASSIFICATION UNCLASSIFIED 2b GROUP Does not apply

3. REPORT TITLE

OPTICAL CONSTANTS OF SILVER AND BARIUM IN THE VACUUM ULTRAVIOLET SPECTRAL REGION

4. DESCRIPTIVE NOTES (Type of report and inclusive dates)

Technical Report, May 1965 to May 1966

5. AUTHOR(S) (Last name, first name, initial)

FISHER, E. I., FUJITA, I., WEISSLER, G. L.

6. REPORT DATE	7a. TOTAL NO. OF PAGES	7b. NO. OF REFS
1 May 1966	97	71

8a. CONTRACT OR GRANT NO. NsG-178-61 b. PROJECT NO. None assigned c. " " d.	9a. ORIGINATOR'S REPORT NUMBER(S) USC-VacUV-108 9b. OTHER REPORT NO(S) (Any other numbers that may be assigned this report) None

10. AVAILABILITY/LIMITATION NOTICES "U.S. Government Agencies may obtain copies of this report directly from DDC. Other qualified DDC users shall request through Physics Dept., Univ. of S. California, Los Angeles."

11. SUPPLEMENTARY NOTES	12. SPONSORING MILITARY ACTIVITY
None	None, see 8a above

13. ABSTRACT The optical properties of evaporated silver and barium films have been investigated in the wavelength range from 1500 to 3000 Å. Reflectance measurements with unpolarized light were made at two angles of incidence, 17.5° and 72.5°, and the components of the complex index of refraction obtained from graphical solutions of the Fresnel equations. The films were prepared in an ultrahigh vacuum reflectometer having a base pressure of about 5×10^{-10} torr. Radiation from a hydrogen glow discharge light source was dispersed by a normal incidence vacuum monochromator which was optically connected to the ultrahigh vacuum system by means of a sapphire window. The energy loss functions, as computed from the optical constants, were compared with published characteristic electron loss data. The complex index of refraction of barium was fitted to a Drude model for which the plasma energy was fixed at 7.42 eV and the damping was allowed to be energy dependent.

DD FORM 1 JAN 64 1473

UNCLASSIFIED

Security Classification